Available online at www.sciencedirect.com
SCIENCE DIRECT®
Journal of Hydrology 279 (2003) 18–42
Journal of Hydrology
www.elsevier.com/locate/jhydrol

Theoretical development and analytical solutions for transport of volatile organic compounds in dual-porosity soils

Mohamed M. Hantush[a,*], Rao S. Govindaraju[b]

[a]*Land Remediation and Pollution Control Division, National Risk Management Research Laboratory, ORD, US EPA, 26 West Martin Luther King Dr, Cincinnati, OH 45268, USA*
[b]*School of Civil Engineering, Purdue University, West Lafayette, IN 47907, USA*

Received 17 April 2002; accepted 14 April 2003

Abstract

Predicting the behavior of volatile organic compounds in soils or sediments is necessary for managing their use and designing appropriate remedial systems to eliminate potential threats to the environment, particularly the air and groundwater resources. In this effort, based on continuity of mass flux, we derive a mass flux boundary condition of the third type in terms of physically based mass transfer rate coefficients, describing the resistance to mass inflow of the soil–air interface, and obtain one-dimensional analytical solutions for transport and degradation of volatile organic compounds in semi-infinite structured soils under steady, unsaturated flow conditions. The advective–dispersive mass balance formulation allows for mobile–immobile liquid phase and vapor diffusive mass transfer, with linear equilibrium adsorption and liquid–vapor phase partitioning in the dynamic and stagnant soil regions. The mass transfer rate coefficients of volatile organic chemicals across the soil–air interface are expressed in terms of solute properties and hydrodynamic characteristics of resistive soil and air-boundary layers. The solutions estimate solute vapor flux from soil surface and describe mobile-phase solute concentration as a function of depth in the soil and time. In particular, solutions were derived for: (1) zero-initial concentration in the soil profile subject to a continuous and pulsed source at the soil surface; and (2) depletion from the soil following an initially contaminated soil profile. Sensitivity analysis with respect to different dimensionless parameters is conducted and the effect on solute concentration and vapor flux of such parameters as volatilization mass transfer velocity relative to infiltration, soil Peclet number, biochemical decay, and diffusive mass transfer into the immobile phase, is plotted and the results are discussed. The mass transfer rate coefficients and the analytical solutions are applied to simulate transport of an example volatile organic compound in an aggregated soil. The simulated results indicate that macropore-aggregate vapor phase diffusion may profoundly impact transport of volatile compounds in aggregated soils.
Published by Elsevier B.V.

Keywords: Transport processes; Aggregrated soil; Volatile organic compound; Model; Mobile–immobile phase; Vapor; Leaching; Mass transfer; Laplace transform

1. Introduction

Gas-phase transport affects the fate and transport of volatile organic chemicals (VOCs) in unsaturated soils and can have important environmental

* Corresponding author.
E-mail address: hantush.mohamed@epa.gov (M.M. Hantush).

0022-1694/03/$ - see front matter Published by Elsevier B.V.
doi:10.1016/S0022-1694(03)00157-4

consequences. Disposal of organic waste in landfills and land treatment systems, accidental chemical spills, and leaky storage tanks, are potential contributors to air and groundwater pollution, by volatilization from the soil surface and downward migration to ground water through the vadose zone. Widespread use of soil fumigants, although useful for increasing crop production, has also contributed to air pollution and groundwater contamination. Understanding the transport and fate of organic chemicals is not only useful for assessing their behavior in the environment, but also in the management of organic waste and agricultural chemicals, and the remediation of VOCs by soil venting or vacuum extraction. In this regard, mathematical models describing the movement and fate of chemicals are effective tools for predicting their behavior in the environment, managing their use and/or disposal, and for the design of effective land treatment and remedial strategies.

This paper presents a mathematical model for transport and degradation of VOCs in three-phase, two-region (aggregated) unsaturated soils. The processes of mobile–immobile phase diffusion (e.g. between macropores and aggregates) of soluble and gaseous phases and volatilization from the soil surface are particularly emphasized. Transport in dual-porosity soils (structured or mobile–immobile phase porous media) is often characterized by early initial breakthrough and an asymmetric concentration profile with extended tailing (Coats and Smith, 1964; van Genuchten and Wierenga, 1976; Gaudet et al., 1977; Rao et al., 1980; Rasmuson and Neretnieks, 1980; DeSmedt and Wierenga, 1984; Valocchi, 1985; Brusseau, 1992). This phenomenon has also been reported in the literature for stratified porous media and fractured media (Grisak and Pickens, 1980, 1981; Tang et al., 1981; Gillham et al., 1984; Güven et al., 1984; Sudicky et al., 1985; Shapiro, 1987; Tang and Aral, 1992; Piquemal, 1993; Li et al., 1994; Hantush and Mariño, 1998a,b). The early initial breakthrough may be the result of the water flow being confined to a fraction of the total pore space due to existing stagnant water regions or pockets occupying the remaining fraction; thus, leading to a faster water flow than that predicted on the basis of flow through the entire pore space. The asymmetric concentration profile and extended tailing may be caused by physical or transport related nonequilibrium, resulting from diffusive mass transfer between the dynamic (mobile) and stagnant (immobile) water regions, and sorption-related nonequilibrium resulting from rate-limited sorption–desorption processes (van Genuchten and Wagenet, 1989; Brusseau et al., 1989; Haggerty and Gorelick, 1995). These studies presented mathematical models in which equilibrium and nonequilibrium sorption–desorption occur at multiple sites, with physical nonequilibrium resulting from mobile–immobile phase transport.

The advent of soil venting or vacuum extraction as a means for the removal of volatile organic compounds and the impact these compounds and agricultural pesticides can have on the environment when released to the atmosphere, has increased the interest in modeling gas phase transport in soils (Jury et al., 1983; Hutzler et al., 1989; Gierke et al., 1990; Brusseau, 1991; Gierke et al., 1992; Yates et al., 1993; Batterman et al., 1995; Johnson et al., 1996; Zaidel et al., 1996; Yates et al., 2000; Hantush et al., 2002). Choy and Reible (2000) provided a compendium of analytical solutions describing volatilization from the soil surface of initially contaminated semi-infinite and finite soil profiles. They also considered stratified initial concentration and multi-layered soil systems, with time-dependent soil–air partition coefficients. The effect of intra-aggregate (liquid) diffusion and rate-limited/instantaneous sorption, on solute vapor transport has also been analyzed (Gierke et al., 1990; Braussea, 1991; Gierke et al., 1992; Hantush et al., 2002). Gierke et al. (1990), however, considered mass transfer resistance at the air–water interface, in which mass transfer from solution to vapor phase is considered rate-limited.

Although the utility of analytical solutions is limited by the simplifying assumptions, they are useful for: (1) elucidating the relative importance of interacting processes; (2) designing and interpreting data from column studies; (3) screening of chemicals; and (4) validating the performance of complex numerical algorithms. The mathematical model formulated in this paper is based on partial differential equations describing mass balance of volatile organics in three-phases and in aggregated soil. The mobile–immobile phase system of equations is shown to be essentially similar to that developed by van Genuchten and Wagenet (1989), however, extended here to transport of VOCs with mobile–immobile phase

diffusion of solute in solution and vapor phases. The latter occurs due to nonequilibrium of liquid phase concentrations in partially saturated mobile and immobile regions. Explicit expressions are derived, which describe soil surface resistance to VOCs' mass flux across the soil–air interface. Further, the equations are solved in a semi-infinite soil profile for three different boundary and initial conditions: (1) zero-initial concentrations with instantaneous flushing of mass from depth of incorporation; (2) zero-initial concentrations and time-dependent and pulsed-type sources introduced at a rate equal to the infiltration rate; and (3) flushing of a contaminated soil profile, with uniform initial concentration in each of the mobile and immobile phases. We later use the solutions to conduct sensitivity analyses and demonstrate their applicability through an example.

2. Mathematical development

2.1. Mass balance formulation

The conceptual framework underlying the model development herein is shown in Fig. 1. Fig. 1(a) shows an overview of the solution domain and an aggregated

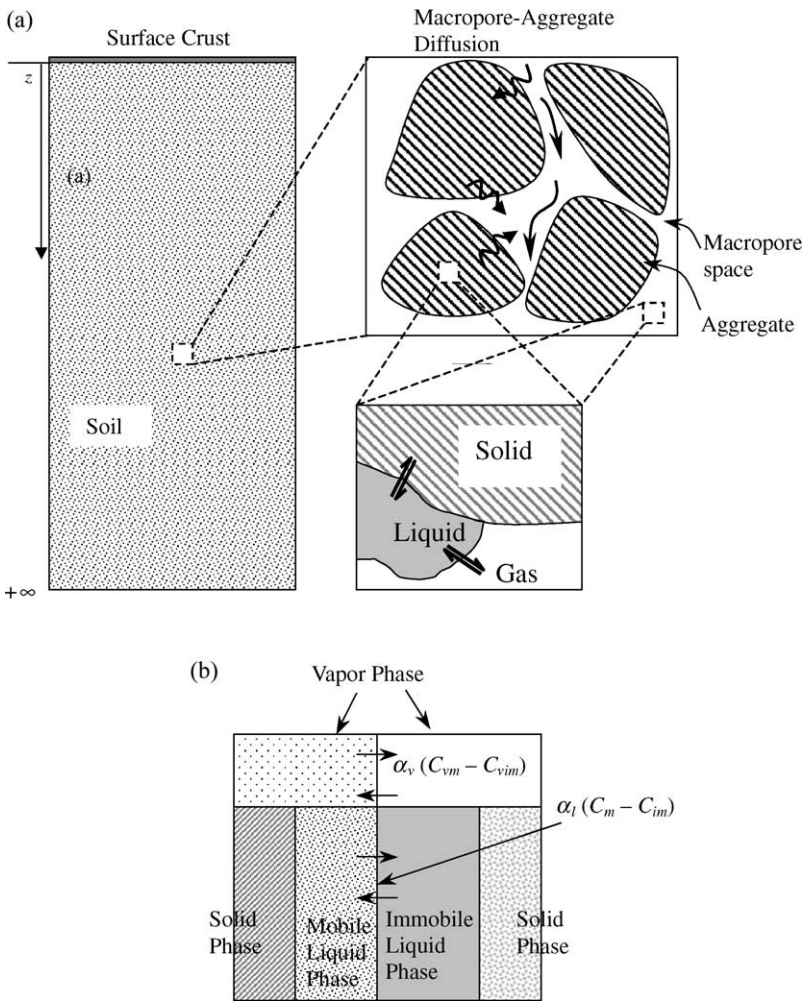

Fig. 1. (a) Illustrations of soil profile and mobile–immobile phase transport in aggregated soil, and (b) conceptual two-region multiphase (liquid, solid, and air) transport model with advection–dispersion normal to the page.

soil, with mobile–immobile phase (macropore-aggregate) transport. Fig. 1(b) shows typical liquid–vapor–solid phases in macropores and aggregates, and related mobile–immobile phase mass transfer. Under unsaturated soil conditions, vapor transport may occur by diffusion between macropores and aggregates through interconnected air-occupied pore space. At contact surfaces between the liquid and solid phase, mass transfer can occur by adsorption and desorption in the macropores and aggregates. In our two-region model, we allow for mobile–immobile phase vapor diffusion and assume that it—as the case of liquid phase diffusion—affects the behavior of VOCs in partially saturated soils.

The two-region model presented here and the analyses that follow are based on these assumptions: (1) equilibrium liquid–vapor partitioning; (2) linear equilibrium liquid–solid phase sorption isotherms; (3) steady-state flow in a semi-infinite and uniform soil profile; (4) mobile–immobile phase mass transfer (liquid and vapor) is limited by a first-order diffusion process; and (5) transport of solute vapor from soil surface (i.e. volatilization) occurs through thin, resistive soil and air-boundary layers (Fig. 2).

Mass balance of volatile solutes in mobile and immobile regions may be described by these equations:

$$\frac{\partial \theta_m C_m}{\partial t} + \frac{\partial \kappa_m C_{vm}}{\partial t} + f_m \rho_b \frac{\partial S_m}{\partial t} = \frac{\partial}{\partial z}\left(\theta_m D_l \frac{\partial C_m}{\partial z} - q C_m\right) + \frac{\partial}{\partial z}\left(\kappa_m D_{vm} \frac{\partial C_{vm}}{\partial z}\right) - \alpha_l (C_m - C_{im}) - \alpha_v (C_{vm} - C_{vim}) - \theta_m k_{lm} C_m - \kappa_m k_{vm} C_{vm} - f_m \rho_b k_{sm} S_m \quad (1)$$

$$\frac{\partial \theta_{im} C_{im}}{\partial t} + \frac{\partial \kappa_{im} C_{vim}}{\partial t} + f_{im} \rho_b \frac{\partial S_{im}}{\partial t} = \alpha_l (C_m - C_{im}) + \alpha_v (C_{vm} - C_{vim}) - \theta_{im} k_{lim} C_{im} - \kappa_{im} k_{vim} C_{vim} - f_{im} \rho_b k_{sim} S_{im} \quad (2)$$

in which C_m and C_{im} are concentrations of solute in solution in mobile and immobile phases, respectively [ML^{-3}]; C_{vm} are C_{vim} are solute vapor concentrations in mobile and immobile regions, respectively [ML^{-3}]; q is soil flow rate per unit area [LT^{-1}]; θ_m is volumetric water content in mobile region; θ_{im} is volumetric water content in immobile region; k_{lm} is first-order liquid phase degradation rate in mobile region [T^{-1}]; k_{lim} is first-order liquid phase degradation rate in immobile region [T^{-1}]; κ_m is volumetric air content in mobile region; κ_{im} is volumetric air content in immobile region; D_l is liquid-phase soil dispersion coefficient [L^2T^{-1}]; k_{vm} is first-order solute vapor degradation rate in mobile region [T^{-1}]; k_{vim} is first-order solute vapor degradation rate in immobile region [T^{-1}]; D_{vm} is gaseous diffusion coefficient in mobile region [L^2T^{-1}]; α_l is first-order mass transfer rate coefficient for liquid phase [T^{-1}]; α_v is first-order mass transfer rate coefficient for vapor phase [T^{-1}]; S_m is sorbed phase concentration in mobile region [MM^{-1}]; S_{im} is sorbed phase concentration in immobile region [MM^{-1}]; f_m is fraction of sorbent in contact with mobile water; ρ_b is soil bulk density [ML^{-3}]; $f_{im} = 1 - f_m$ is fraction of sorbent in contact with immobile water; k_{sm} is first-order degradation rate of adsorbed phase in mobile region [T^{-1}]; k_{sim} is first-order degradation rate of adsorbed phase in immobile phase [T^{-1}]; t is time [T]; and z is distance [L].

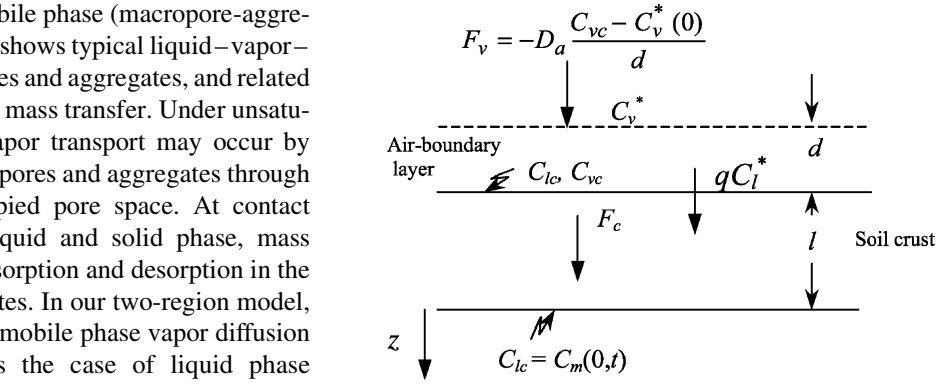

Fig. 2. A schematic diagram of soil–air interface model.

These equations apply to both soil regions as a whole irrespective of whether the sorption process is rate-limited or at equilibrium, and they account for first-order vapor mass transfer between the mobile and immobile regions.

We consider linear equilibrium sorption isotherms

$$S_m = K_d C_m, \qquad S_{im} = K_d C_{im} \quad (3)$$

and assume that vapor concentration is linearly related to solution concentration (Henry's law),

$$C_{vm} = K_H C_m \qquad C_{vim} = K_H C_{im} \quad (4)$$

in which K_d is the soil–water distribution coefficient [L^3M^{-1}]; and K_H is the dimensionless Henry's constant. Substituting Eqs. (3) and (4) for S_m, S_{im}, C_{vm}, and C_{vim}, into Eqs. (1) and (2), one obtains for steady state flow in a uniform medium these equations

$$\theta_m R_m \frac{\partial C_m}{\partial t} = \theta_m D_m \frac{\partial^2 C_m}{\partial z^2} - q\frac{\partial C_m}{\partial z} - \theta_m R_m k_m C_m - \theta_m \alpha (C_m - C_{im}) \quad (5)$$

$$\theta_{im} R_{im} \frac{\partial C_{im}}{\partial t} = \theta_m \alpha (C_m - C_{im}) - \theta_{im} R_{im} k_{im} C_{im} \quad (6)$$

in which the effective solution phase dispersion coefficient D_m is given by

$$D_m = D_l + \frac{\kappa_m D_{vm} K_H}{\theta_m} \quad (7)$$

and the effective liquid-phase first-order rate transfer coefficient, and effective liquid-phase degradation rates in the mobile and immobile regions, respectively, are given by

$$\alpha = \frac{\alpha_l + K_H \alpha_v}{\theta_m} \quad (8)$$

$$k_m = \left\{1 + \frac{f_m \rho_b K_d}{\theta_m}\frac{k_{sm}}{k_{lm}} + \frac{\kappa_m K_H}{\theta_m}\frac{k_{vm}}{k_{lm}}\right\}\frac{1}{R_m} k_{lm} \quad (9)$$

$$k_{im} = \left\{1 + \frac{f_{im} \rho_b K_d}{\theta_{im}}\frac{k_{sim}}{k_{lim}} + \frac{\kappa_{im} K_H}{\theta_{im}}\frac{k_{vim}}{k_{lim}}\right\}\frac{1}{R_{im}} k_{lim} \quad (10)$$

where

$$R_m = 1 + \frac{\kappa_m K_H + f_m \rho_b K_d}{\theta_m}, \qquad R_{im} = 1 + \frac{\kappa_{im} K_H + f_{im} \rho_b K_d}{\theta_{im}} \quad (11)$$

R_m and R_{im} are the retardation factors in the mobile and immobile phases, respectively.

Dividing both sides of Eqs. (5) and (6) by θ_m and adding the latter to the former yields

$$R_m \frac{\partial C_m}{\partial t} + \beta R_{im} \frac{\partial C_{im}}{\partial t} + \beta k_{im} R_{im} C_{im} = -\frac{\partial F_m}{\partial z} - k_m R_m C_m \quad (12)$$

in the mobile phase, and

$$\beta R_{im} \frac{\partial C_{im}}{\partial t} + \beta k_{im} R_{im} C_{im} = \alpha (C_m - C_{im}) \quad (13)$$

in the immobile phase, where

$$F_m(z,t) = -D_m \frac{\partial C_m(z,t)}{\partial z} + u C_m(z,t) \quad (14)$$

in which $\beta = \theta_{im}/\theta_m$; and $u = q/\theta_m$ is the average pore-water velocity in the dynamic soil region [LT^{-1}]. Its worth noting that if sufficient pressure gradient is applied to induce gas advection at a flux rate of v (positive along the z axis), then, in this case, $u = (q + vK_H)/\theta_m$. In essence, Eqs. (12) and (13) can describe gas advection during soil venting or vacuum extraction (Brusseau, 1991). For nonvolatile compounds Eqs. (13) and (14), although remain similar in form, reduce to those originally developed by van Genuchten and Wagenet (1989), with the parameters Eqs. (8)–(11) redefined accordingly. Hantush and Mariño (1998a) arrived at a similar system, which describes transport of nonvolatile reactive contaminant in a two-layer stratified system, under saturated flow conditions.

In the absence of soil surface resistance, the following initial and boundary conditions may be considered:

$$C_{im}(z,0), \qquad C_m(z,0) = 0 \quad (15a)$$

$$-\kappa_m D_{vm} \frac{\partial C_{vm}(0,t)}{\partial z} = -D_a \frac{C_{vm}(0,t) - C_v^*(t)}{d} \quad (15b)$$

$$-\theta_m D_l \frac{\partial C_m(0,t)}{\partial z} + q C_m(0,t) = M_o \delta(t) + q C_l^*(t) \quad (15c)$$

$$\frac{\partial C_m}{\partial z}, \frac{\partial C_{im}}{\partial z} = 0, \; z \to \infty \quad (15d)$$

in which $C_v^*(t)$ is solute vapor concentration above the air-boundary layer [ML^{-3}]; $C_l^*(t)$ is liquid solute concentration entering soil surface at a constant rate q (e.g. precipitation or irrigation) [ML^{-3}]; D_a is the vapor diffusion coefficient in free air [L^2T^{-1}]; M_o is initial mass per unit area within depth of incorporation [ML^{-2}]; $\delta(t)$ is the Dirac delta function [T^{-1}]. Depending on the actual system under consideration, the two boundary-source terms on the right-hand-side of Eq. (15c) need not be accounted for simultaneously. For example, in the absence of an external source, $C_l^*(t) = 0$.

The total mass flux at the soil–air interface is given by $F_m(0,t)$, which is the sum of Eqs. (15b) and (15c). Assuming zero vapor concentration above the surface ($C_v^*(t)=0$), it is given by

$$\theta_m F_m(0,t) = -\sigma C_m(0,t) + M_o\delta(t) + qC_l^*(t) \tag{16}$$

where

$$\sigma = K_H D_a/d \tag{17}$$

in which we used the Henry's law relation $C_{vm}(z,t) = K_H C_m(z,t)$, and $C_v^*(t)=0$. Eq. (16) describes volatilization from soil surface, advective liquid phase solute source, and rapid flushing of solute mass from a thin topsoil layer (depth-of-incorporation). The parameter σ describes the rate of solute vapor mass transfer at the soil-air interface (i.e. volatilization mass transfer velocity). We note that Eqs. (16) and (17) ignore soil resistance to mass transfer and account only for air resistance.

For applications related to land treatment systems, contaminated sediments may be sealed from the environment by a cap layer that provides resistance to solute vapor mass transfer in addition to minimizing infiltration rates significantly. Surface crusts and compacted topsoil layers also present interface resistance to diffusive and advective mass transfer (Yates et al., 2000). In the presence of such layers, solute flux through the layers may be described by a third-type boundary condition, expressed in terms of unknown rate transfer parameter (Yates et al., 2000). The rate transfer parameter is usually estimated by calibration, since no expressions are currently available to estimate this parameter. In the following section we derive a general form for the flux boundary condition (16) in terms of mass transfer rate coefficients that describe the resistance to solute mass flow at the soil–air interface, as shown in Fig. 2. The coefficients extend the utility of the analytical solutions to transport of VOCs in soil with a distinct, thin resistive layer at the surface.

2.2. Effective mass transfer rate coefficient

Fig. 2 shows the two-layer system of soil crust and air-boundary layer under consideration. In deriving a general form for the flux boundary condition (16), we make two main assumptions. First, the residence time in the resistive soil layer is too small for degradation to significantly impact the solute concentration. Secondly, the sorptive process is too slow relative to the rate of fluid flow in the layer, for adsorption to affect liquid phase concentration. Based on these assumptions, transport of solute in vapor and soluble phases through the resistive soil layer may be described by this equation:

$$\theta_c\frac{\partial C_{lc}}{\partial t} + \kappa_c\frac{\partial C_{vc}}{\partial t} = \frac{\partial}{\partial z}\left(\kappa_c D_{vc}\frac{\partial C_{vc}}{\partial z}\right) + \frac{\partial}{\partial z}\left(\theta_c D_{lc}\frac{\partial C_{lc}}{\partial z}\right) - q\frac{\partial C_{lc}}{\partial z} \tag{18}$$

in which C_{lc} is liquid-phase concentration in the resistive soil layer [ML^{-3}]; C_{vc} is solute vapor concentration in the resistive layer [ML^{-3}]; θ_c is volumetric water content of the resistive layer [L^3L^{-3}]; κ_c is volumetric air content of the resistive layer [L^3L^{-3}]; D_{vc} is resistive-layer gaseous diffusion coefficient [L^2T^{-1}]; and D_{lc} is dispersion coefficient in the resistive layer [L^2T^{-1}]. For convenience, we redefine the origin of z to be at the upper boundary of the layer whose thickness is l [L]. The use of equilibrium vapor-soluble phase partitioning relationship $C_{vc} = K_H C_{lc}$ in Eq. (18) leads to a mass balance equation expressed in terms of the soluble concentration,

$$(\theta_c + K_H\kappa_c)\frac{\partial C_{lc}}{\partial t} = \frac{\partial}{\partial z}\left(\theta_c D_c\frac{\partial C_{lc}}{\partial z}\right) - q\frac{\partial C_{lc}}{\partial z} \tag{19}$$

in which the effective liquid-phase dispersion is given by

$$D_c = D_{lc} + K_H\frac{\kappa_c}{\theta_c}D_{vc} \tag{20}$$

Comparison of the order of magnitudes of the dispersive and advective terms on the right-hand-side of Eq. (19) with the time-derivative term on left-hand-side reveals that

$$\left|(\theta_c + K_H\kappa_c)\frac{\partial C_{lc}}{\partial t}\right| \ll \left|\frac{\partial}{\partial z}\left(\theta_c D_c\frac{\partial C_{lc}}{\partial z}\right)\right|,\ \left|q\frac{\partial C_{lc}}{\partial z}\right| \tag{21}$$

if

$$t \gg (l^2/D_c)\left(1 + K_H\frac{\kappa_c}{\theta_c}\right), l(\theta_c + K_H\kappa_c)/q \tag{22}$$

in which l is the thickness of resistive layer [L]. Under either condition, the partial derivative term with respect to time can be neglected relative to the dispersive and/or advective terms on the right-hand side of Eq. (19), and the concentration in the solution phase, in this case, is at quasi-steady state. For purely diffusive transport, the first constraint in Eq. (22) is required. Based on condition (22), the partial derivative with respect to time can be dropped and Eq. (19) is simplified to

$$\frac{\partial}{\partial z}\left(\theta_c D_c \frac{\partial C_{lc}}{\partial z}\right) - q\frac{\partial C_{lc}}{\partial z} = 0 \tag{23}$$

In which we retained the partial derivative terms to emphasize that C_{lc} still is a function of t. In Appendix A we solve Eq. (23) subject to these boundary conditions (see Fig. 2)

$$-\kappa_c D_{vc}\frac{\partial C_{vc}(0,t)}{\partial z} = -D_a\frac{C_{vc}(0,t) - C_v^*(t)}{d} \tag{24a}$$

$$-\theta_c D_{lc}\frac{\partial C_{lc}(0,t)}{\partial z} + qC_{lc}(0,t) = qC_l^*(t) \tag{24b}$$

Note that although Eq. (23) is essentially an ordinary differential equation, its solution subject to the time-dependent boundary conditions (24a) and (24b) actually is a function of time. The solution of Eqs. (23), (24a) and (24b) is shown in Appendix A to yield this flux boundary condition

$$\theta_m F_m(0,t) = -\sigma C_m(0,t) + \mu_v C_v^*(t) + \mu_l C_l^*(t) + M_o\delta(t) \tag{25}$$

where

$$\sigma = \frac{K_H\frac{q}{e^{P_c}-1}}{K_H + \frac{d}{D_a}q\frac{e^{P_c}}{e^{P_c}-1}} \tag{26}$$

$$\mu_v = \frac{q\frac{e^{P_c}}{e^{P_c}-1}}{K_H + \frac{d}{D_a}q\frac{e^{P_c}}{e^{P_c}-1}} \tag{27}$$

$$\mu_l = q^2\frac{d}{D_a}\frac{\frac{e^{P_c}}{e^{P_c}-1}}{K_H+\frac{d}{D_a}q\frac{e^{P_c}}{e^{P_c}-1}} \tag{28}$$

in which $P_c = ql/(\theta_c D_c)$ is the resistive-layer Peclet number. These mass transfer rate parameters are based on the quasi-steady-state transport and negligible impact of degradation and adsorption within the resistive soil layer.

Recall that Eq. (16) applies to the case of no resistive soil layer, in which case, by taking the limits $l \to 0$ and $P_c \to 0$ in Eqs (27)–(28), respectively, one obtains the rather expected results: $\sigma = K_H D_a/d$; $\mu_v = D_a/d$; and $\mu_l = q$. For purely diffusive transport, we have $q = 0$, $\lim_{q\to 0}[q/(e^{P_c}-1)] = \theta_c D_c/l$, and Eqs. (26)–(28) become

$$\sigma = \frac{\theta_c D_c}{l}\frac{K_H}{K_H + \frac{d}{D_a}\frac{\theta_c D_c}{l}},$$
$$\mu_v = \frac{\theta_c D_c}{l}\frac{1}{K_H + \frac{d}{D_a}\frac{\theta_c D_c}{l}}, \qquad \mu_l = 0 \tag{29}$$

Eqs. (26)–(28) describe the rate of mass transfer across the soil–air interface in wet soils, with the solute liquid-vapor partitioning, fluid advection, gas diffusion, longitudinal dispersion, and geometry accounted for explicitly.

2.3. Solutions

We limit the solutions herein to the mobile-phase concentrations, C_m, and consider first, the case of a source at soil surface with zero initial concentrations throughout a semi-infinite soil profile, and second, a soil profile with uniform mobile–immobile initial concentrations subject to infiltration and no source at soil surface. Since Eqs. (12) and (13) are linear, a solution for a combination of both source at soil surface and uniform initial concentrations can be obtained by superposition of individual solutions. We will consider a time-dependent source, instantaneous flushing of mass from soil surface (i.e. from depth of incorporation), and a pulsed-type source. We use the general flux boundary condition (25) to obtain solutions for exponentially decaying solute concentration entering soil surface, $C_l^*(t) = C^* e^{-a_1 t}$ (Govindaraju et al., 1996), however, for zero vapor concentration above the air-boundary layer, $C_v^*(t) = 0$. Solutions for a constant or exponentially decaying vapor concentration above the air-boundary layer can be easily deduced.

2.3.1. Time dependent source with zero-initial concentration

The solution of Eqs. (12) and (13) subject to initial condition (15a) and boundary conditions (15d) and (25) is obtained using Laplace transformation, the details of which are shown in Appendix B. We express the solution in terms of the dimensionless variables:

$$C_m^*(z^*,t^*) = C_m(z,t)/C_0;\quad \gamma = (\mu_l/q)C^*/C_0;\quad t^* = t/T_r;\quad z^* = z/h;\quad \lambda = \sigma/q;\quad \alpha^* = \alpha T_r/R_m;\quad k_m^* = k_m T_r;\quad k_{im}^* = k_{im}T_r;\quad \varepsilon = \beta R_{im}/R_m;\quad a_1^* = a_1 T_r;\quad K^* = (k_{im}^* + \alpha^*/\varepsilon) \tag{30}$$

where $C_0 = M_o/(qT_r) = M_o/(h\theta_m R_m)$ is a characteristic initial liquid-phase solute concentration within soil depth h; h is a characteristic soil depth, chosen arbitrarily [L]; and $T_r = hR_m/u$ is the residence time.

$$C_m^*(z^*,t^*) = \sqrt{P}F(z^*,t^*) + \sqrt{P}\gamma\int_0^{t^*} e^{-a_1^*(t^*-\tau)} h_1(z^*,\tau)\psi(\tau)\,d\tau \tag{31}$$

where $F(z^*,t^*) = \sqrt{T_r}f(z,t)$; $f(z,t)$ is given in Appendix B

$$F(z^*,t^*) = \frac{\alpha^*}{\sqrt{\varepsilon}}\int_0^{t^*}\sqrt{\frac{\tau}{t^*-\tau}} I_1\left[\frac{2\alpha^*}{\sqrt{\varepsilon}}\sqrt{(t^*-\tau)\tau}\right] \times e^{-K^*(t^*-\tau)} g^*(z^*,\tau)\,d\tau + g^*(z^*,t^*) \tag{32}$$

$$g^*(z^*,\tau) = e^{-[k_m^*+\alpha^*]\tau} h^*(z^*,\tau) \tag{33}$$

$$h_1(z^*,\tau) = \exp\left(-\left[k_m^* + \frac{\varepsilon\alpha^*(k_{im}^*-a_1^*)}{\alpha^*+\varepsilon(k_{im}^*-a_1^*)}\right]\tau\right) h^*(z^*,\tau) \tag{34}$$

$$h^*(z^*,\tau) = \exp\left(-\frac{P\tau}{4}\left(\frac{z^*}{\tau}-1\right)^2\right)\left\{\frac{1}{\sqrt{\pi\tau}} - \frac{\sqrt{P}}{2}(2\lambda+1) \times \exp\left(\frac{P\tau}{4}\left(\frac{z^*}{\tau}+(2\lambda+1)\right)^2\right) \times \operatorname{erfc}\left[\frac{\sqrt{P\tau}}{2}\left(\frac{z^*}{\tau}+(2\lambda+1)\right)\right]\right\} \tag{35}$$

$$\psi(\tau) = 1 - \exp\left(-\left\{\frac{\alpha^{*2}\tau}{\varepsilon(k_{im}^*-a_1^*)+\alpha^*} + \left[\frac{\epsilon(k_{im}^*-a_1^*)+\alpha^*}{\varepsilon}\right](t^*-\tau)\right\}\right) \times \sum_{m=1}^{\infty}\left\{\left(\frac{\varepsilon\alpha^{*2}}{[\varepsilon(k_{im}^*-a_1^*)+\alpha^*]^2}\frac{\tau}{t^*-\tau}\right)^{m/2} \times I_m\left[\frac{2\alpha^*}{\sqrt{\varepsilon}}\sqrt{(t^*-\tau)\tau}\right]\right\} \tag{36}$$

where $g^*(z^*,t^*) = \sqrt{T_r}g_1(z,t)$; $g_1(z,t)$ is given in Appendix B; $P = uh/D_m$ is the Peclet number; $I_m[x]$ is the modified Bessel function of the first kind of order m. Lindstrom and Stone (1974) derived another form for Eq. (36):

$$\psi(\tau) = \exp\left(-\left\{\frac{\alpha^{*2}\tau}{\varepsilon(k_{im}^*-a_1^*)+\alpha^*} + \left[\frac{\varepsilon(k_{im}^*-a_1^*)+\alpha^*}{\varepsilon}\right] \times (t^*-\tau)\right\}\right)\sum_{m=0}^{\infty}\left\{\left(\frac{[\varepsilon(k_{im}^*-a_1^*)+\alpha^*]^2}{\varepsilon\alpha^{*2}}\frac{t^*-\tau}{\tau}\right)^{m/2} \times I_m\left[\frac{2\alpha^*}{\sqrt{\varepsilon}}\sqrt{(t^*-\tau)\tau}\right]\right\} \tag{37}$$

From the speed of convergence standpoint, they recommended that the integral in Eq. (32) be broken into two parts from $\tau=0$ to $\tau=t^*/\{1+\varepsilon\alpha^{*2}/[\varepsilon(k_{im}^*-a_1^*)+\alpha^*]^2\}$ with $\psi(\tau)$ given by Eq. (36) and from $\tau = t^*/\{1+\varepsilon\alpha^{*2}/[\varepsilon(k_{im}^*-a_1^*)+\alpha^*]^2\}$ to $\tau=t^*$ with $\psi(\tau)$ defined by Eq. (37). The following approximation may be useful for evaluating Eq. (35) (Abramowitz and Stegun, 1972):

$$h^*(z^*,\tau) = \frac{\exp\left(-\frac{P}{4\tau}(\tau-z^*)^2\right)}{\sqrt{\pi\tau}}\frac{z^*}{z^*+(2\lambda+1)\tau}, \quad \text{if } \frac{\sqrt{P\tau}}{2}\left(\frac{z^*}{\tau}+(2\lambda+1)\right) > 3 \tag{38}$$

Eq. (31) describes liquid-phase solute concentrations in the mobile region as a function of depth in soil and time. The first term on the right-hand-side accounts for instantaneous flushing of mass from soil surface, and the second term describes the contribution of exponentially decaying (or a constant) source at soil surface introduced at a rate equal to the infiltration rate.

Vapor flux across the soil–air interface without vapour source can be estimated from this equation:

$$F_v(t) = -\sigma C_m(0,t) \tag{39}$$

which in a dimensionless form can be written as

$$F_v^*(t^*) = -\lambda C_m^*(0,t^*) \tag{40}$$

where

$$F_v^*(t^*) = \frac{T_r}{M_o} F_v(t) \tag{41}$$

2.3.2. Pulse-type source with zero-initial concentration

For pulse-type application of the chemical in solution at the source,

$$C_l(t) = \begin{cases} C^* & 0 \le t \le t_1 \\ 0 & t > t_1 \end{cases} \tag{42}$$

The solution for $C_m^*(z^*,t^*)$, by virtue of the linearity of Eqs. (12) and (13), is thus given by superposition:

For $t^* > t_1^*$,

$$\begin{aligned} C_m^*(z^*,t^*) = \sqrt{P}F(z^*,t^*) + \sqrt{P}\gamma\Bigg\{ & \int_0^{t^*} h_1(z^*,\tau;a_1=0) \\ & \times \psi(\tau;a_1=0)\mathrm{d}\tau - \int_0^{t^*-t_1^*} h_1(z^*,\tau;a_1=0) \\ & \times \psi(\tau;a_1=0)\mathrm{d}\tau \Bigg\} \end{aligned} \tag{43}$$

and for $t^* < t_1^*$,

$$\begin{aligned} C_m^*(z^*,t^*) = \sqrt{P}F(z^*,t^*) + \sqrt{P}\gamma & \int_0^{t^*} h_1(z^*,\tau;a_1=0) \\ & \times \psi(\tau;a_1=0)\mathrm{d}\tau \end{aligned} \tag{44}$$

in which $h_1(z^*,\tau;a_1=0)$ and $\psi(\tau;a_1=0)$ are given by Eqs. (34) and (36) or (37) evaluated at $a_1=0$, and t_1^* is the dimensionless time for duration of pulse.

2.3.3. Initially contaminated profile

The initial and boundary conditions of a soil profile, with uniform initial concentration and no source applied at the soil surface ($C_l^*, C_v^* = 0, M_o = 0$) are

$$C_m(z,0) = C_m^0, \quad C_{im}(z,0) = C_{im}^0 \tag{45a}$$

$$-\kappa_m D_v \frac{\partial C_{vm}(0,t)}{\partial z} = -D_a \frac{C_{vm}(0,t)}{d} \tag{45b}$$

$$-\theta_m D_l \frac{\partial C_m(0,t)}{\partial z} + qC_m(0,t) = 0 \tag{45c}$$

$$\frac{\partial C_m}{\partial z}, \frac{\partial C_{im}}{\partial z} = 0, \qquad z \to \infty \tag{45d}$$

Concentration above air layer is also assumed zero, $C_v^* = 0$. Combining Eqs. (45b) and (45c) with Eq. (14) leads to

$$\theta_m F_m(0,t) = -\sigma C_m(0,t) \tag{46}$$

in which σ is give by Eq. (26) for soil–air resistance. The solution of the partial differential Eqs. (12) and (13) subject to Eqs. (45a), (45d), and (46) is obtained in Appendix C, using Laplace transformation, which in a dimensionless form is

$$\begin{aligned} C_m^*(z^*,t^*) = & -(\lambda+1)\sqrt{P}\{\gamma_1 \Psi_1(z^*,t^*) \\ & + \gamma_2 \Psi_2(z^*,t^*)\} + \gamma_1 \Phi_1(t^*) \\ & + \gamma_2 \Phi_2(t^*) \end{aligned} \tag{47}$$

where

$$\begin{aligned} \Phi_1(t^*) &= e^{-K^* t^*} \frac{m_1 e^{m_1 t^*} - m_2 e^{m_2 t^*}}{m_1 - m_2}, \\ m_{1,2} &= -\frac{\kappa^*}{2} \pm \frac{1}{2}\sqrt{\kappa^{*2} + 4\frac{\alpha^{*2}}{\varepsilon}} \end{aligned} \tag{48}$$

$$\Phi_2(t^*) = \alpha^* e^{-K^* t^*} \frac{e^{m_1 t^*} - e^{m_2 t^*}}{m_1 - m_2} \tag{49}$$

$$\begin{aligned} \Psi_1(z^*,t^*) = & \frac{m_1}{m_1 - m_2} \int_0^{t^*} e^{-(K^* - m_1)(t^* - \tau)} \\ & \times h_1(z^*,\tau;a_1 = K^* - m_1) \\ & \times \psi(\tau;a_1 = K^* - m_1)\mathrm{d}\tau \\ & - \frac{m_2}{m_1 - m_2} \int_0^{t^*} e^{-(K^* - m_2)(t^* - \tau)} \\ & \times h_1(z^*,\tau;a_1 = K^* - m_2) \\ & \times \psi(\tau;a_1 = K^* - m_2)\mathrm{d}\tau \end{aligned} \tag{50}$$

$$\Psi_2(z^*,t^*) = \frac{\alpha^*}{m_1-m_2}\left\{\int_0^{t^*} e^{-(K^*-m_1)(t^*-\tau)} \times h_1(z^*,\tau;a_1=K^*-m_1) \times \psi(\tau;a_1=K^*-m_1)\mathrm{d}\tau - \int_0^{t^*} e^{-(K^*-m_2)(t^*-\tau)} \times h_1(z^*,\tau;a_1=K^*-m_2) \times \psi(\tau;a_1=K^*-m_2)\mathrm{d}\tau\right\} \quad (51)$$

where $h_1(z^*,\tau;a_1=r)$ is given by Eq. (34) with r substituted for a_1; and $\psi(\tau;a_1=r)$ is given by Eqs. (36) or (37) with r substituted for a_1. The dimensionless variables above are defined by

$$C_{\mathrm{m}}^*(z^*,t^*) = C_{\mathrm{m}}/C_{\mathrm{avg}};$$

$$C_{\mathrm{avg}} = (\theta_{\mathrm{m}}/\theta)C_{\mathrm{m}}^0 + (\theta_{\mathrm{im}}/\theta)C_{\mathrm{im}}^0;$$

$$\gamma_1 = C_{\mathrm{m}}^0/C_{\mathrm{avg}}; \qquad \gamma_2 = C_{\mathrm{im}}^0/C_{\mathrm{avg}}; \quad (52)$$

$$\kappa^* = k_{\mathrm{m}}^* - k_{\mathrm{im}}^* + \left(\frac{\varepsilon-1}{\varepsilon}\right)\alpha^*$$

in which α^*, k_{m}^*, k_{im}^*, ϵ, K^*, z^*, and t^* are defined earlier; $\theta = \theta_{\mathrm{im}} + \theta_{\mathrm{m}}$ is the soil volumetric water content; and C_{avg} is weighted-average initial concentration in soil.

Eq. (47) describes redistribution and depletion of mobile-phase solution concentrations in a structured or aggregated soil profile starting with a uniform initial concentration in each phase. The first (integral) term on the right-hand-side accounts for the contribution of initial concentration in the mobile water, and the second term describes the contribution of initial concentration in the stagnant water.

Vapor flux, F_{v}, is given by Eq. (39), which in dimensionless form is expressed also as in Eq. (40), $F_{\mathrm{v}}^*(t^*) = -\lambda C_{\mathrm{m}}^*(0,t^*)$, where C_{m}^* is redefined here to be $C_{\mathrm{m}}/C_{\mathrm{avg}}$; and

$$F_{\mathrm{v}}^*(t^*) = \frac{F_{\mathrm{v}}(t)}{qC_{\mathrm{avg}}} \quad (53)$$

3. Parameter sensitivity

Fig. 3(a) shows $C_{\mathrm{m}}(z^*,t^*)$ at $z^*=1$ versus t^* plotted on log-scale, for the dimensionless parameters:

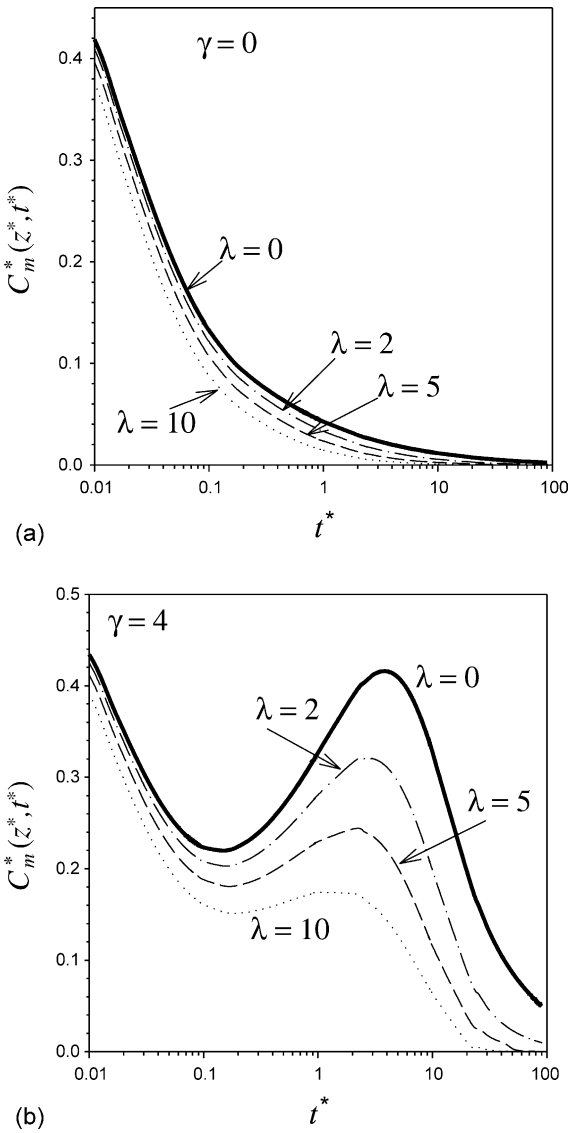

Fig. 3. Dimensionless mobile solution concentration versus dimensionless time at $z^*=1$ for $\lambda = 0$, 2, 5, and 10: (a) $\gamma = 0$, (b) $\gamma = 4$. ($P = 0.01$, $\alpha^* = 5$, $\varepsilon = 0.5$, $a_1^* = 0.2$, $k_{\mathrm{m}}^* = k_{\mathrm{im}}^* = 0$).

$\gamma = 0$, $P = 0.01$, $\alpha^* = 5$, $\varepsilon = 0.5$, $k_{\mathrm{im}}^* = 0$, $k_{\mathrm{m}}^* = 0$, and $\lambda = 0$, 2, 5, and 10. This case corresponds to rapid (instantaneous) flushing of solute mass from the surface. Although not shown in the plot, the concentrations increase rapidly to peak values at $t^* < 0.01$ before declining to near zero values at $t^* = 100$. As expected, the dimensionless concentration decreases with increasing λ, since mobile-phase

concentration decreases with increasing rate of vapor mass transfer away from the soil surface. Fig. 3(b) shows the contribution of a source of magnitude $\lambda = 4$, exponentially decaying at a dimensionless rate $a_1^* = 0.2$. This source produces a second peak concentration in the simulated breakthrough curve, much more delayed than that produced by the rapid flushing of mass from soil surface. The simulated peak dimensionless concentration is significantly reduced when λ increases from 0 to 10, with the concentration generally decreasing with increasing λ.

Fig. 4(a) shows simulated dimensionless vapor flux $F_v^*(t^*)$ at soil surface following instantaneous flushing of solute mass from the soil surface, for $\lambda = 0.5$, 2, 5, and 10. Negative values imply the flux is from soil surface to atmosphere; i.e. in the negative z direction. The vapor flux generally increases with λ, but diminishes in time and eventually approaches zero following leaching of initial mass deep in the soil by advection and dispersion. For exponentially decaying liquid-phase solute source of magnitude $\gamma = 4$, the vapor flux levels off and slightly increases over an extended period of time before declining to zero, as Fig. 4(b) shows. The effect of solute entering soil surface is to maintain vapor flux through the surface for a finite period in time, until source concentration diminishes.

Figs. 5(a) and (b) show dimensionless vapor flux $F_v^*(0, t^*)$ for the case of instantaneous flushing of solute mass from soil surface without source at the soil surface ($\gamma = 0$), and with an exponentially decaying source ($\gamma = 2$, $a_1^* = 0.2$), respectively. In each case, we used these dimensionless parameters: $P = 0.01$, $\lambda = 2, k_m^*, k_{im}^* = 0, \varepsilon = 5, \alpha^* = 0.05, 0.5, 5$, and 15. In both cases, the greater the dimensionless rate of mass transfer α^*, the smaller the dimensionless vapor flux initially, for $t^* < 0.1$. However, $F_v^*(t^*)$ approaches zero more gradually with greater α^* and drops to zero relatively faster for smaller values of α^*. The spread of the solute mass between the mobile and immobile phases produced by diffusive mass transfer increases with α^*, leading to a reduced vapor concentration gradient at the interface, thereby a reduced vapor flux from the soil surface. At later times, diffusion of the solute mass from the immobile phase to the mobile region provides further but a limiting source of vapor available for mass transfer across the soil–air interface. The impact of exponentially decaying source

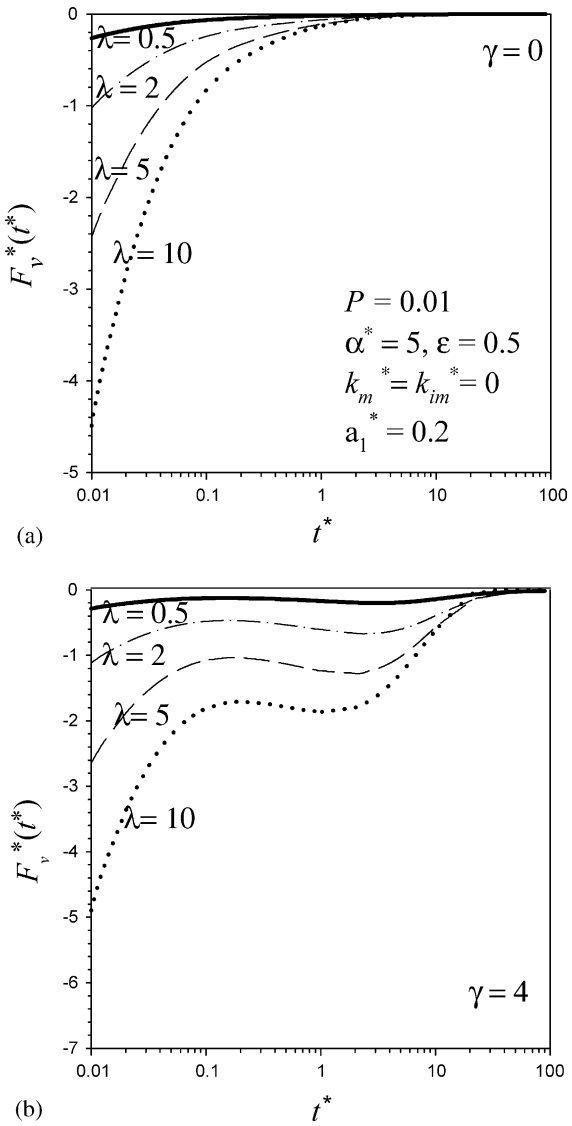

Fig. 4. Dimensionless vapor flux versus dimensionless time for $\lambda =$ 0.5, 2, 5, and 10: (a) $\gamma = 0$, (b) $\gamma = 4$ and $a_1^* = 0.2$. ($P = 0.01$, $\alpha^* = 5$, $\varepsilon = 0.5$, $k_m^* = k_{im}^* = 0$).

concentration at the soil interface on the simulated vapor flux in Fig. 5(b) is similar to that of Fig. 4(b).

The effect of the Peclet number P on the dimensionless vapor flux is shown in Fig. 6, for the case of rapid flushing of M_o. The soil is assumed uniform with the parameters: $\lambda = 1$, $k_m^*, k_{im}^* = 0$, $\varepsilon = 0$, $\alpha^* = 0$, and $P = 0.1$, 1, 5, and 40. The dimensionless vapor flux $F_v^*(t^*)$ increases with P for small t^*, but decreases with this parameter for larger

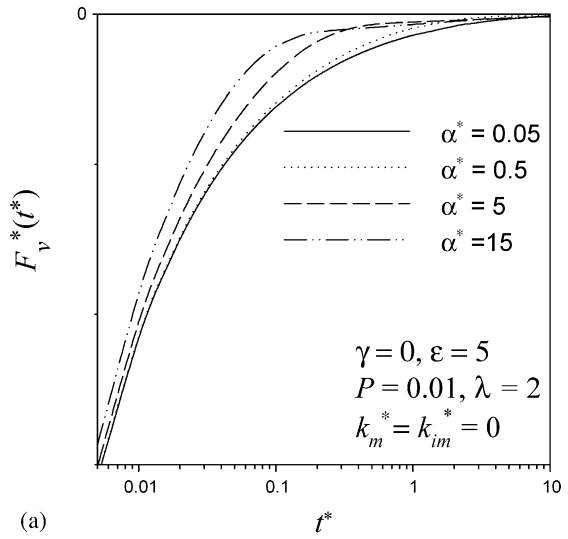

Fig. 5. Dimensionless vapor flux versus dimensionless time for $\alpha^* = 0.05$, 0.5, 5, and 15: (a) $\gamma = 0$, (b) $\gamma = 2$ and $a_1^* = 0.2$. ($P = 0.01$, $\varepsilon = 5$, $\lambda = 2$, $k_m^* = k_{im}^* = 0$).

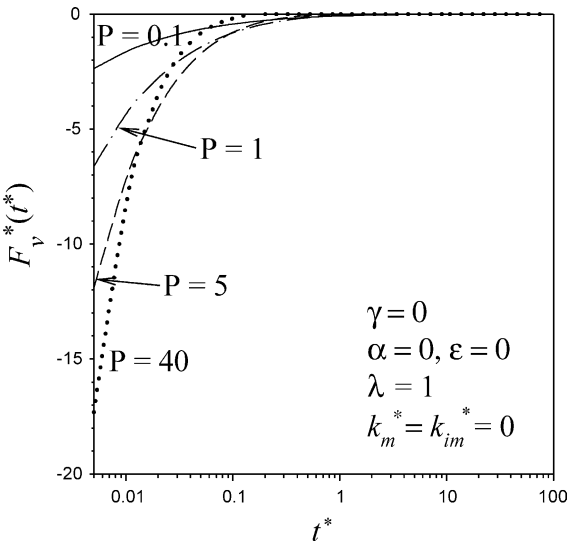

Fig. 6. Dimensionless vapor flux versus dimensionless time for $P = 0.1$, 1, 5, and 40. ($\gamma = 0$, $\alpha^* = 0$, $\varepsilon = 0$, $\lambda = 1$, $k_m^* = k_{im}^* = 0$).

t^*, where $F_v^*(t^*)$ approaches zero relatively faster for larger P. Initially, dispersion dampens the concentration gradient at the soil surface resulting in the decrease of $F_v^*(t^*)$ with P, whereas at later t^*, the concentration gradient at the soil surface is smaller for larger P where advection dominates dispersion and the initial solute mass would have been flushed away more rapidly from the soil surface, thereby resulting in smaller vapor flux for greater P.

To elucidate the role of biochemical decay in the immobile phase as a potential sink, we consider the hypothetical case of degradation limited to the immobile phase (i.e. intra-aggregate) and ignore losses in the mobile phase (i.e. macropores). Fig. 7 shows breakthrough plots at $z^* = 5$ of dimensionless concentrations, and vapor flux for $k_{im}^* = 0$, 0.2, 1, and 10. The source is limited to initial mass within depth of incorporation. The following parameters are assumed: $\alpha^* = 1$, $\lambda = 1$, $k_m^* = 0$, $\varepsilon = 0.5$, and $P = 0.01$. The dimensionless breakthrough concentrations at $z^* = 5$ is initially invariant with the dimensionless decay rate in the immobile phase, k_{im}^*, but decrease with increasing values of this parameter at later dimensionless times. Although not shown, the variation of the dimensionless concentration with k_{im}^* appears earlier as the dimensionless rate transfer parameter α^* increases from 1 to 10. This indicates that degradation in the immobile phase has no immediate impact on the breakthrough concentrations until sufficient time has elapsed for diffusive mass transfer into the immobile phase to take effect. Thus, biochemical losses in the immobile phase are limited by the rate of mass transfer when degradation in the mobile phase is negligible. For small t^*, the simulated dimensionless vapor flux $F_v^*(t^*)$ shows insignificant variation with k_{im}^*, as shown in Fig. 7(b). Similarly, although not shown in a figure, $F_v^*(t^*)$ is more

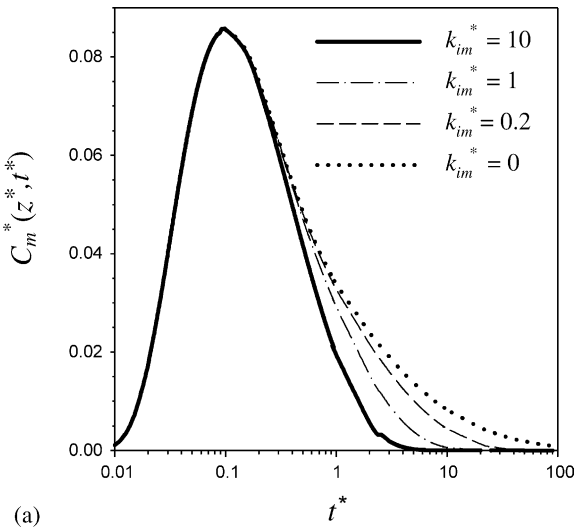

Fig. 7. Dimensionless: (a) mobile solution concentration at $z^* = 5$, (b) vapor flux, for $k_m^* = 0$, $k_{im}^* = 0$, 0.2, 1, and 10. ($\gamma = 0$, $P = 0.01$, $\alpha^* = 1$, $\varepsilon = 0.5$, $\lambda = 1$).

sensitive to k_{im}^* as α^* increases. In general, $F_v^*(t^*)$ decreases as k_{im}^* increases.

Fig. 8(a)–(c) show F_v^* variation with t^* for $\alpha^* =$ 0, 0.1, 1, and 5, for three distinct cases of initially contaminated soil profile in which fraction of immobile phase is assumed to be $\theta_{im}/\theta = 0.6$. Fig. 8(a) simulates the case of initially contaminated immobile zone only, $\gamma_1 = 0$ and $\gamma_2 = C_{im}^0/\{(\theta_{im}/\theta)C_{im}^0\} = 1.67$, and using the following dimensionless parameters: $P = 0.01$, $\varepsilon = 1.5$, $\lambda =$ 5, $k_m^* = k_{im}^* = 0$. The absolute value of F_v^* is shown to increase initially to a peak value, then declines and approach zero at larger t^*. In this scenario, the immobile phase acts as the only source of solute to the mobile phase. The increase in the upward vapor flux is the result of a build-up in vapor concentration gradient at the soil surface, produced by initially greater solute diffusion from the immobile region to the mobile phase, thus, leading to increase in F_v^*. As the concentration gradient between the mobile and immobile phases declines in time and solute is being leached from the soil surface deep in the profile, F_v^* would eventually decrease as diffusive mass transfer into the mobile zone diminishes in time and mobile solution concentration continues to be reduced from the soil profile by leaching. In general, absolute F_v^* increases with α^*; however, at relatively large t^* (say, greater than 20), this behavior is reversed. The other two cases of uniform and equal initial concentration in both mobile and immobile phases and zero initial concentration in the immobile phase, respectively, are shown in Fig. 8(b) and (c). In both cases, absolute F_v^* decreases monotonically with t^*, albeit at different rates over the time scales $0.01 \leq t^* \leq 100$. Fig. 8(b) shows that absolute F_v^*, generally, increases with α^*. This, however, is not the case for zero-initial immobile-phase concentration, where absolute F_v^* decreases with increasing α^* for $t^* <$ 1. Such behavior is expected, since initially, greater α^* implies greater mass transfer by diffusion from the mobile zone and eventually reduced mobile-phase solute vapor concentration and gradient at the soil surface; thus, smaller F_v^*. An interesting feature is that for the zero-initial immobile phase concentration (Fig. 8(c)) as α^* increases, the behavior of F_v^* with t^* becomes visibly characterized by two distinct slopes corresponding to the rate of decrease of absolute F_v^* with t^*; an initially sharp decline followed by a much more gradual one. Reversed mass transfer from the immobile phase back into the mobile phase may be responsible for such a behavior. For sufficiently large t^*, absolute F_v^* appears to increase with α^*.

Fig. 9 shows simulated dimensionless mobile-phase concentration profiles at $t^* = 1$ for $\alpha^* = 0$, 1, and 5, starting with a uniform initial concentration, $\gamma_1 = \gamma_2 = 1$. C_m^* increases with α^* because of

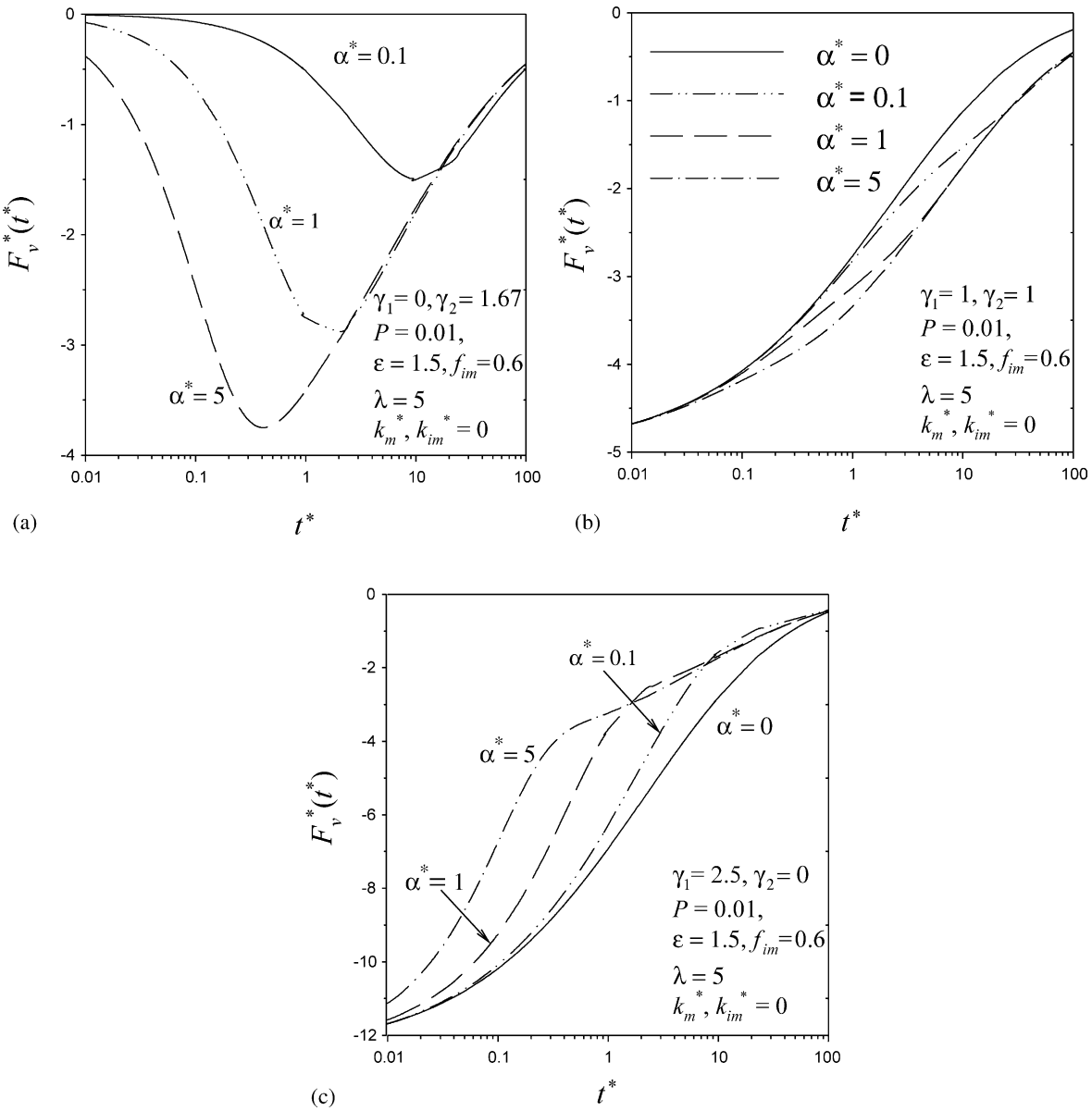

Fig. 8. Dimensionless vapor flux versus time following initially contaminated soil profile and no other source for $\alpha^* = 0$, 0.1, 1, and 5: (a) $\gamma_1 = 0$, $\gamma_2 = 1.67$, (b) $\gamma_1 = 1$, $\gamma_2 = 1$, (c) $\gamma_1 = 2.5$, $\gamma_2 = 0$. ($f_{im} = 0.6$, $P = 0.01$, $\epsilon = 1.5$, $\lambda = 5$, $k_m^* = k_{im}^* = 0$).

the increase with this parameter of the solute mass transfer by diffusion from the immobile phase to the mobile phase. Fig. 10 shows variation of dimensionless mobile-phase concentration with λ, in which C_m^* at depths closer to the surface decreases significantly with increasing values of this parameter.

4. Application

Table 1 lists example soil and chemical parameters and relationships for estimating diffusion, dispersion, and degradation rate. The selected values for K_H, K_{oc}, λ_{im}, and λ_m resemble those of the pesticide Heptachlor

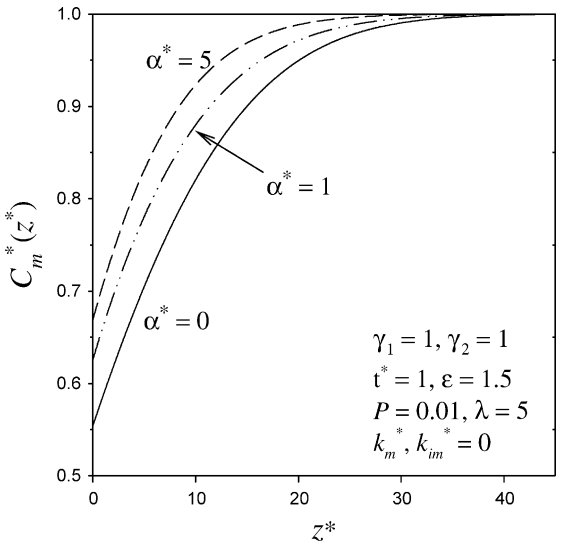

Fig. 9. Dimensionless mobile solution concentration profiles at $t^* = 1$ for $\alpha^* = 0$, 1, and 5. ($\gamma_1 = 1$, $\gamma_2 = 1$, $P = 0.01$, $\varepsilon = 1.5$, $\lambda = 5$, $k_m^* = k_{im}^* = 0$).

(Rao et al., 1985). The relatively large half-life of 2000 d is indicative of the low degradation rate. Degradation in the vapor phase is ignored. This example simulates two transport scenarios in a semi-infinite profile: (1) leaching following rapid flushing of initial mass of $M_o = 2 \times 10^{-4}$ kg/m^2 from

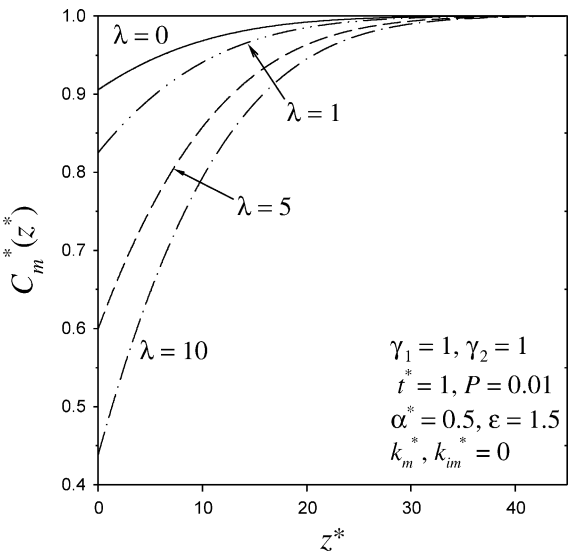

Fig. 10. Dimensionless mobile solution concentration profiles at $t^* = 1$ for $\lambda = 0$, 1, 5, and 10. ($\gamma_1 = 1$, $\gamma_2 = 1$, $P = 0.01$, $\alpha^* = 0.5$, $\varepsilon = 1.5$, $k_m^* = k_{im}^* = 0$).

Table 1
List of example parameters

Parameter	Value
M_o (kg/m^2)	2×10^{-4}
C_m^0, C_{im}^0 (kg/m^3)	10^{-5}
λ_m, λ_{im} (d)	2000
K_H	1.45×10^{-1}
K_{oc} (m^3/kg)	24
f_{oc} (kg/kg)	2×10^{-3}
D_a (m^2/d)	4.32×10^{-1}[a]
D_w (m^2/d)	4×10^{-5}
α_d (cm)[b]	5
α_c (cm)[c]	1
q (cm/d)	1
d (cm)	0.5[a]
l (cm)	1
r (cm)	0.4
ρ_b (kg/m^3)	1.2×10^3
n_m (cm^3/cm^3)	0.4
n_{im} (cm^3/cm^3)	0.3
θ_m (cm^3/cm^3)	0.2
θ_{im} (cm^3/cm^3)	0.15, 0.3
n_c (cm^3/cm^3)	0.4
θ_c (cm^3/cm^3)	0.2
D_l (m^2/d)	2.5×10^{-3}[b]
D_c (m^2/d)	2.33×10^{-3}[c]
σ (m/d)	4.2×10^{-2}[d]

[a] Suggested by Jury et al. (1983), d = 0.5 cm for bare soil surfaces.
[b] $D_l = \alpha_d q/\theta_m + D_w(\theta_m^{10/3}/n_m^2)$, α_d is the soil dispersivity [L].
[c] $D_c = \alpha_c q/\theta_c + D_w(\theta_c^{10/3}/n_c^2) + K_H(\kappa_c/\theta_c)D_{vc}$, $D_{vc} = D_a\kappa_c^{10/3}/n_c^2$, α_c is the surface crust dispersivity [L].
[d] Eq. (26). $D_{vm} = D_a\kappa_m^{10/3}/n_m^2$, $D_{vim} = D_a\kappa_{im}^{10/3}/n_{im}^2$ $k_{lm} = \ln(2)/\lambda_m$, $k_{lim} = \ln(2)/\lambda_{im}$.

soil surface (Figs. 11 and 12); and (2) leaching following an initially contaminated soil with a uniform concentration of 10^{-5} kg/m^3 (Fig. 13). A steady-state infiltration rate $q = 1$ cm/d is assumed to occur through a surface crust of thickness $l = 1$ cm and an aggregated soil with a total porosity of 0.7 and aggregate radius of 0.4 cm. The results plotted in Figs. 11 and 12 are obtained by evaluating the first term on the right-hand-side of Eq. (B36) or Eq. (31) (recall, $\gamma = 0$). Volatilization velocity $\sigma = 0.042$ m/d is obtained from Eq. (26) and the example soil crust parameters in Table 1. In this particular example, we have $(l^2/D_c)(1 + K_H\kappa_c/\theta_c) = 0.05$ d and $l(\theta_c + K_H\kappa_c)/q = 0.23$ d, which, with some confidence, implies that the use of Eq. (26) may be justified for $t \geq 1$ d. We use this relationship for estimating the liquid-phase mass transfer coefficient for spherical

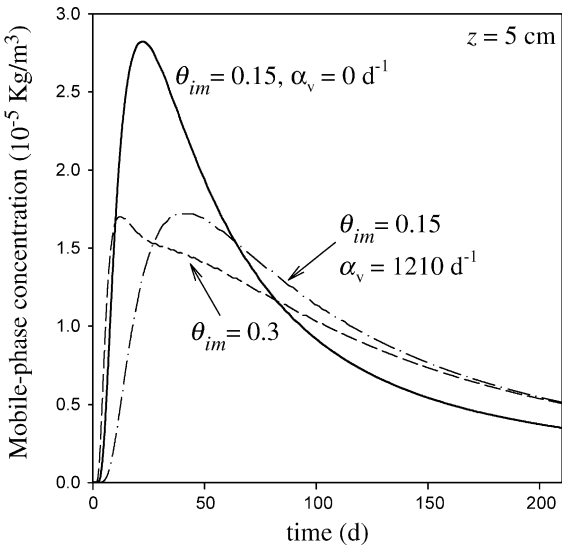

Fig. 11. Simulated mobile solution concentration following rapid flushing of an initial mass from soil surface, for saturated ($\theta_{im} = 0.3$) and partially saturated aggregates ($\theta_{im} = 0.15$), with connected ($\alpha_v = 1210\ d^{-1}$) and disconnected ($\alpha_v = 0\ d^{-1}$) mobile–immobile air-pore space.

aggregate (Brausseau, 1991, and references therein):

$$\alpha_l = 15\frac{D_{im}}{r^2}, \qquad D_{im} = D_w\frac{\theta_{im}^{10/3}}{n_{im}^2} \tag{54}$$

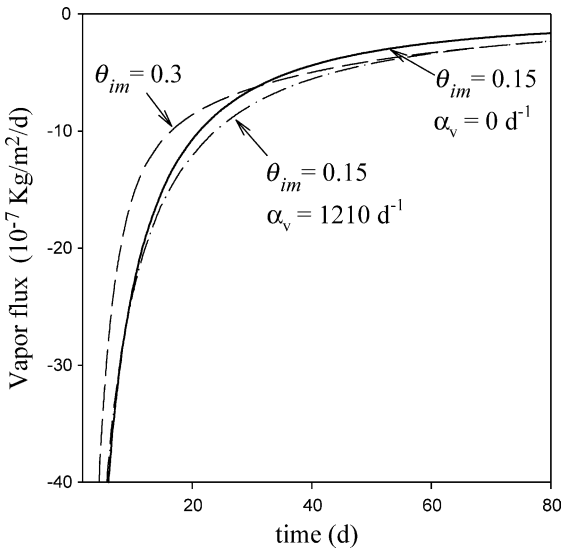

Fig. 12. Simulated vapor flux following rapid flushing of an initial mass from soil surface, for saturated ($\theta_{im} = 0.3$) and partially saturated aggregates ($\theta_{im} = 0.15$), with connected ($\alpha_v = 1210\ d^{-1}$) and disconnected ($\alpha_v = 0\ d^{-1}$) mobile–immobile air-pore space.

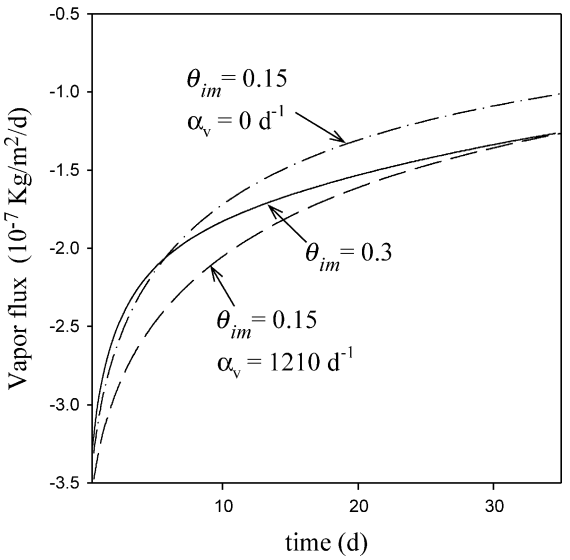

Fig. 13. Simulated vapor flux following leaching of initially contaminated soil with uniform concentration, for saturated ($\theta_{im} = 0.3$) and partially saturated aggregates ($\theta_{im} = 0.15$), with connected ($\alpha_v = 1210\ d^{-1}$) and disconnected ($\alpha_v = 0\ d^{-1}$) mobile–immobile air-pore space.

in which D_w is the diffusion coefficient in water [L^2T^{-1}]; and r is the aggregate radius [L]. Similarly, by assuming interconnected vapor-occupied macropore and micropore spaces, the rate of vapor mass transfer between the macropores and the aggregates may be described by this relationship:

$$\alpha_v = 15\frac{D_{vim}}{r^2}, \qquad D_{vim} = D_a\frac{\kappa_{im}^{10/3}}{n_{im}^2} \tag{55}$$

We simulate three different cases: (1) saturated aggregates and partially saturated macropores, (2) partially saturated macropores and aggregates with interconnected mobile—immobile vapor phase, (3) partially saturated macropores and aggregates with a disconnected mobile—immobile vapor phase. In the first case, the solute vapor is limited to the mobile phase, whereas in the second case, solute vapor exists in both the aggregates and macropores and vapor mass transfer occurs by diffusion between the two regions. In the third case, solute vapor exists in both regions but without significant interactions (i.e. both regions are disconnected). The retardation factors (Eq. (11)) are estimated using the approximation $f_m = \theta_m/(\theta_m + \theta_{im})$, which has been shown to be successful in previous applications (Brausseau, 1991, and references

therein). For a fully saturated aggregate ($\theta_{im} = 0.3$), Eqs (54) and (55) estimate $\alpha_l = 2.26\ d^{-1}$, and $\alpha_v = 0\ d^{-1}$, and for partially saturated aggregate ($\theta_{im} = 0.15$), we have $\alpha_l = 0.11\ d^{-1}$, and $\alpha_v = 1210\ d^{-1}$. Eq. (55) predicts vapor mass transfer at a rate of four orders of magnitude greater than the rate of liquid phase mass transfer.

Fig. 11 shows simulated mobile-phase concentration in time at depth 5 cm below soil following rapid flushing of an initial mass. Breakthrough is predicted earlier, with a more rapid increase toward a peak value for saturated aggregates when compared to partially saturated aggregates with a connected macropore–micropore vapor phase ($\alpha_v = 1210\ d^{-1}$). The solution predicts a significantly greater peak concentration and smaller concentrations at later times for the case of a partially saturated, disconnected vapor phase ($\theta_{im} = 0.15$, $\alpha_v = 0$). Vapor mass transfer between the macropores and aggregates by diffusion has the effect of retarding solute movement in the soil and producing a greater spread of the solute relative to the case of no vapor interactions between the two regions (Fig. 11). Fig. 12 shows computed vapor flux as a function of time at the soil surface. The solution predicts greater vapor flux—negative values implying vapor flux from the soil to the air—with decreasing saturation of aggregates for a relatively long period of time. However, and although not shown in the figure, the computed vapor flux at $t < 2$ d is greater for saturated aggregates than for the case of partial saturation. For saturated aggregates ($\theta_{im} = 0.3$) the residence time, T_r, for soil depth 0.1 cm is equal to 2.3 d. Initially, and within this window of time, a fraction of the solute initial mass still is remaining within this depth, with potentially more solute vapor available for diffusion from the surface than for partially saturated aggregates ($\theta_{im} = 0.15$). In the latter, however, vapor diffusion into the partially saturated micropores (or aggregates) reduces vapor concentration at the interface, and the dampened concentration gradients at the interface therefore lead to smaller vapor fluxes. However, at times much greater than the residence time, much of the initial mass would be flushed deeper in the soil, and vapor diffusion from the aggregate back into the soil macropores would then sustain a greater vapor flux from soil surface than would be the case for saturated aggregates. The solution computes asymptotically similar vapor flux for both the saturated and partially saturated aggregate scenarios; e.g., at time greater than 60 d in this example. For this particular application, Ignoring vapor transfer between macropores and aggregates ($\theta_{im} = 0.15$, $\alpha_v = 0$)--or equivalently, a disconnected macropore-aggregate vapor phase--slightly overestimates vapor flux earlier, say, $t \leq 10$ d, while underestimates it significantly at later times.

Fig. 13 shows simulated vapor flux at the soil surface following an initially wetted soil profile with a uniform concentration of 10^{-5} kg/m^3, using the data in Table 1 and Eq. (C13) or Eq. (47). The solution predicts less vapor flux from the soil surface with increased aggregate saturation for at least 30 d. The relatively greater vapor flux from the surface for the partially saturated aggregates is the result of vapor-phase diffusion to macropores, even though solution phase diffusion to macropores increases with increasing saturation of aggregates. The computed vapor flux in Fig. 13 is greater when the solute vapor is allowed to diffuse between the aggregates and micropores than for the case of no interactions (i.e. $\alpha_v = 0\ d^{-1}$). If indeed the micropore void space and macropores are connected, then solutions, which ignore aggregate-macropore vapor diffusion, may either underestimate vapor flux from the soil surface or produce artifact parameters during calibration.

5. Summary and conclusions

The disposal of VOCs in landfills and land treatment systems or their use as soil fumigants in agriculture has increased the interest in using mathematical models as tools for predicting the behavior of these chemicals in the environment and estimating the potential for air pollution and groundwater contamination. A coupled system of partial differential equations is presented, which describes mass balance of VOCs in three-phases (liquid, air, and solid) in a dual-porosity (aggregated or structured) soil under unsaturated flow conditions. The coupled transport and fate equations are essentially similar in form to those

developed by van Genuchten and Wagenet (1989), however, extended here to the vapor phase, including mobile–immobile phase vapor diffusion. Physically based algebraic expressions were developed, which describe the resistance to solute mass flux at the soil surface. The expressions, valid when certain conditions are satisfied, related mass transfer rate coefficients to the solute chemical properties and hydrodynamic characteristics of the surface crust and air-boundary layer. In effect, a boundary condition of third type (i.e. Cauchy boundary condition) has been developed for liquid-vapor phase mass flow through a resistive soil–air interface. Semi-infinite domain analytical solutions were developed for three different cases: (1) zero-initial concentration and leaching and volatilization from soil surface following rapid flushing of mass from soil surface; (2) zero-initial concentrations and time dependent and pulsed-type source introduced at a rate equal to infiltration rate; and (3) flushing of a contaminated soil profile with uniform initial concentration. The solutions predict concentration as a function of depth in soil and time, and the resulting vapor flux at the soil (sediment)-air interface (i.e. volatilization rate). The processes of vapor flux from the soil surface and mobile–immobile phase mass transfer were particularly emphasized. Simulations based on the solution in a dimensionless form showed the synergistic effect at different time scales (relative to residence time) of such processes as advection relative to hydrodynamic dispersion, volatilization from soil surface relative to infiltration, biochemical decay, and macropore-aggregate diffusion, on dimensionless breakthrough concentration, dimensionless vapor flux from the soil surface, and concentration profile. Applicability of the analytical solutions and mass transfer rate coefficients was demonstrated through an example. The results showed that macropore-aggregate vapor phase diffusion impacts significantly the predicted mobile solution concentrations and vapor flux from the soil surface. The expressions for the mass transfer rate coefficients and the analytical solutions may be useful for management of VOCs in agriculture and designing disposal sites.

Acknowledgements

The US Environmental Protection Agency through its Office of Research and Development funded and managed the research described here through in-house efforts. It has not been subjected to Agency review and therefore does not necessarily reflect the views of the Agency, and no official endorsement should be inferred. Special thanks to Mark Goltz and the anonymous reviewer for their constructive review comments. The manuscript benefited from their review comments.

Appendix A

For convenience, we replace the partial derivatives with ordinary derivative, and rewrite Eq. (23) with ξ as the spatial coordinate as

$$\theta_c D_c \frac{d^2 C_{lc}}{d\xi^2} - q\frac{dC_{lc}}{d\xi} = 0, \qquad 0 \le \xi \le l \tag{A1}$$

in which $\xi = 0$ is at soil–air interface (i.e. top of the resistive soil layer in Fig. 2). The soil moisture and dispersion are assumed to be uniform in the resistive soil layer. Integrating Eq. (A1) from 0 to ξ yields

$$\theta_c D_c \frac{dC_{lc}}{d\xi} - qC_{lc} + \{-\theta_c D_c \frac{dC_{lc}}{d\xi} + qC_{lc}\Big|_{\xi=0}\} = 0 \tag{A2}$$

or

$$\theta_c D_c \frac{dC_{lc}}{d\xi} - qC_{lc} + F_c = 0 \tag{A3}$$

in which F_c is the equivalent liquid-phase flux at the soil surface, given by the two terms between parentheses in Eq. (A2) [$ML^{-2}T^{-1}$]. Thus, by adding the boundary fluxes Eqs. (24a) and (24b), we have

$$F_c(t) = \frac{D_a}{d}\left[C_v^*(t) - K_H C_{lc}(0,t)\right] + qC_l^*(t) \tag{A4}$$

in which we used $C_{vc} = K_H C_{lc}$. Irrespective of the dependence of C_{lc} and F_c on time, the solution of the ordinary differential Eq. (A3) is given by

$$C_{lc}(\xi,t) = \exp\left(\frac{q}{\theta_c D_c}\xi\right) C_{lc}(0,t) + \frac{1}{q}F_c(t) \times \left(1 - \exp\left(\frac{q}{\theta_c D_c}\xi\right)\right) \tag{A5}$$

in which $C_{lc}(0,t)$ is liquid phase concentration at $\xi = 0$ (Fig. 2). Note that we have restored the dependence on time notation between parentheses. Evaluating Eq. (A5) at $\xi = l$ and noting that $C_{lc}(l,t) = C_m(0,t)$ (Fig. 2) leads to this expression for $F_c(t)$

$$F_c(t) = -q\frac{C_m(0,t) - e^{P_c}C_{lc}(0,t)}{e^{P_c} - 1} \tag{A6}$$

where

$$P_c = \frac{ql}{\theta_c D_c} \tag{A7}$$

is the liquid-phase Peclet number associated with the soil resistive layer. Solving Eq. (A4) for $C_{lc}(0,t)$ and substituting into Eq. (A6) and solving for F_c leads to

$$F_c(t) = -\sigma C_m(0,t) + \mu_v C_v^*(t) + \mu_l C_l^*(t) \tag{A8}$$

where σ, μ_v, and μ_l are given by Eqs. (26)–(28), respectively. The contribution of initial mass within depth of incorporation can be added to yield this general boundary flux equation

$$\theta_m F_m(0,t) = F_c(t) + M_o\delta(t) \tag{A9}$$

For purely diffusive mass transport through the air layer, we have $q = 0$, thus,

$$\lim_{q\to 0} F_c(t) = \frac{\theta_c D_c}{l}\frac{1}{K_H + (d/D_a)(\theta_c D_c/l)} \times \left[C_v^*(t) - K_H C_m(0,t)\right] \tag{A10}$$

Appendix B

The Laplace transforms of Eq. (12), after substituting Eq. (14) for $F_m(z,t)$, and Eq. (13) are

$$pR_m\tilde{C}_m(z;p) - R_m C_m(z,0) + \beta R_{im}p\tilde{C}_{im}(z;p) - \beta R_{im}C_{im}(z,0) + \beta k_{im}R_{im}\tilde{C}_{im}(z;p) = D_m\frac{d^2\tilde{C}_m(z;p)}{dz^2} - u\frac{d\tilde{C}_m(z;p)}{dz} - k_m R_m\tilde{C}_m(z;p) \tag{B1}$$

$$\beta R_{im}p\tilde{C}_{im}(z;p) - \beta R_{im}C_{im}(z,0) + \beta k_{im}R_{im}\tilde{C}_{im}(z;p) = \alpha\left(\tilde{C}_m(z;p) - \tilde{C}_{im}(z;p)\right) \tag{B2}$$

where the Laplace transform of a function $f(z,t)$ is

$$\tilde{f}(z;p) = \int_0^\infty f(z,t)e^{-pt}\,dt \tag{B3}$$

Boundary conditions (15d) and (25) with $C_l^*(t) = C^* e^{-a_l t}$ and $C_v^*(t) = 0$ in the Laplace domain are given by

$$\frac{d\tilde{C}_m}{dz}, \frac{d\tilde{C}_{im}}{dz} = 0, \qquad z\to\infty \tag{B4}$$

$$\theta_m\tilde{F}_m(0;p) = -\sigma\tilde{C}_m(0;p) + M_o + \frac{\mu_l C^*}{p + a_1} \tag{B5}$$

Eq. (B2) can be solved for $\tilde{C}_{im}(z;p)$ in terms of $\tilde{C}_m(z;p)$,

$$\tilde{C}_{im}(z;p) = \frac{\alpha}{\beta R_{im}(p + k_{im}) + \alpha}\tilde{C}_m(z;p) \tag{B6}$$

In which we used the initial condition (15a). Combining Eqs. (B6) with (B1) to eliminate $\tilde{C}_{im}(z;p)$ and substituting Eq. (15a) for $C_m(z,0)$ and $C_{im}(z,0)$ leads to this ordinary differential equation:

$$\frac{d^2\tilde{C}_m(z;p)}{dz^2} - \frac{u}{D_m}\frac{d\tilde{C}_m(z;p)}{dz} - \frac{R_m}{D_m} \times\left\{p + k_m + \frac{1}{R_m}\frac{\beta R_{im}(p + k_{im})\alpha}{\beta R_{im}(p + k_{im}) + \alpha}\right\}\tilde{C}_m(z;p) = 0 \tag{B7}$$

The solution of this equation subject to boundary conditions (B4) and (B5) is obtained immediately,

$$\tilde{C}_m(z;p) = \frac{1}{\sigma + \theta_m D_m m_2(p)} \times\left[M_o + \frac{\mu_l C^*}{p + a_1}\right]e^{m_1(p)z} \tag{B8}$$

where

$$m_1(p) = (1/2)\left[u/D_m - \sqrt{u^2/D_m^2 + 4(R_m/D_m)\left\{p + k_m + \frac{(\beta R_{im}/R_m)(p + k_{im})\alpha}{\beta R_{im}(p + k_{im}) + \alpha}\right\}}\right] \tag{B9}$$

and

$$m_2(p) = (1/2)\left[u/D_m + \sqrt{u^2/D_m^2 + 4(R_m/D_m)\left\{ p + k_m + \frac{(\beta R_{im}/R_m)(p+k_{im})\alpha}{\beta R_{im}(p+k_{im}) + \alpha} \right\}} \right] \quad \text{(B10)}$$

We start by rewriting Eq. (B8) as

$$\tilde{C}_m(z;p) = \left(M_o + \frac{\mu_1 C^*}{p + a_1} \right) \frac{\tilde{f}[z; s(p)]}{\theta_m \sqrt{D_m R_m}} \quad \text{(B11)}$$

where

$$\tilde{f}[z; s(p)] = \frac{e^{\left\{ u/2D_m - \sqrt{R_m/D_m}\sqrt{d^* + s(p)} \right\} z}}{b^* + \sqrt{d^* + s(p)}} \quad \text{(B12)}$$

in which

$$s(p) = p + K + \frac{a}{p+K} \quad \text{(B13)}$$

$$K = k_{im} + \frac{\alpha}{\beta R_{im}}, \qquad a = -\frac{\alpha^2}{\beta R_{im} R_m} \quad \text{(B14)}$$

$$d^* = \frac{u^2}{4R_m D_m} + k_m + \frac{\alpha}{R_m} - K, \quad \text{(B15)}$$

$$b^* = \frac{u}{2\sqrt{R_m D_m}} \left(2\frac{\sigma}{v} + 1 \right)$$

The right-hand side of Eq. (B12) an be inverted following the procedure of Lindstrom and Narasimham (1973),

$$f(z,t) = \mathfrak{L}^{-1}\{\tilde{f}(z;p)\}$$

$$= e^{-Kt} \frac{\partial}{\partial t} \int_0^t J_0[2\sqrt{a(t-\tau)\tau}] g(z,\tau) d\tau \quad \text{(B16)}$$

where

$$g(z,t) = \mathfrak{L}_s^{-1}\{\tilde{f}(z;s)\}$$

$$= \mathfrak{L}_s^{-1}\left\{ \frac{e^{\left\{ u/2D_m - \sqrt{R_m/D_m}\sqrt{d^* + s} \right\} z}}{b^* + \sqrt{d^* + s}} \right\}$$

$$= e^{(u/2D_m)z - d^* t} \mathfrak{L}_s^{-1}\left\{ \frac{e^{-a^*\sqrt{s}}}{b^* + \sqrt{s}} \right\} \quad \text{(B17)}$$

and

$$a^* = \sqrt{\frac{R_m}{D_m}} z \quad \text{(B18)}$$

in which $J_0[x]$ is the zero-order Bessel function of the first kind; and $\mathfrak{L}^{-1}$ is the Laplace inverse transform operator with respect to the parameter s. The evaluation of Eq. (B17) is readily available from Roberts and Kaufman (1966),

$$g(z,t) = e^{(uz/2D_m) - d^* t} \left\{ \frac{e^{-\frac{a^{*2}}{4t}}}{\sqrt{\pi t}} - b^* e^{a^* b^* + b^{*2} t} \times \operatorname{erfc}\left[\frac{a^*}{2\sqrt{t}} + b^* \sqrt{t} \right] \right\} \quad \text{(B19)}$$

Eq. (B16) can be written after the substitution for a in the integrand as

$$f(z,t) = e^{-Kt} \frac{\partial}{\partial t} \int_0^t I_0\left[\frac{2\alpha}{\sqrt{\beta R_{im} R_m}} \sqrt{(t-\tau)\tau} \right] \times g(z,\tau) d\tau \quad \text{(B20)}$$

in which $J_0[ix] = I_0[x]$ is employed. $I_0[x]$ is the zero-order modified Bessel function of the first kind. It can be simplified further using Leibnitz' rule and $I_0[0] = 1$ to yield

$$f(z,t) = \int_0^t \frac{\alpha}{\sqrt{\beta R_{im} R_m}} \sqrt{\frac{\tau}{t-\tau}} I_1\left[\frac{\alpha}{\sqrt{\beta R_{im} R_m}} \sqrt{(t-\tau)\tau} \right] \times g(z,\tau) d\tau + e^{-Kt} g(z,t) \quad \text{(B21)}$$

in which the Bessel identity $d/dt\{I_0[u(t)]\} = I_1[u(t)]\, du/dt$ is used; and $I_1[x]$ is the first-order modified Bessel function of the first kind. Also, note that in applying the Leibnitz' rule, $g(z,0) = 0$, which can be verified using the familiar identity $\lim_{t\to 0} g(z,t) = \lim_{s\to\infty} s\tilde{f}(z;s)$ and evaluating this limit. Eq. (B21) can be written in a more compact form after substituting for a^*, b^*, and d^* into Eq. (B19) and completing a square,

$$f(z,t) = \frac{\alpha}{\sqrt{\beta R_{im} R_m}} \int_0^t \sqrt{\frac{\tau}{t-\tau}} I_1\left[\frac{2\alpha}{\sqrt{\beta R_{im} R_m}} \sqrt{(t-\tau)\tau} \right] \times e^{-K(t-\tau)} g_1(z,\tau) d\tau + g_1(z,t) \quad \text{(B22)}$$

where

$$g_1(z,\tau)=\exp\left(-\left[k_m+\frac{\alpha}{R_m}\right]\tau-\frac{R_m}{4D_m\tau}\left(\frac{u\tau}{R_m}-z\right)^2\right)\left\{\frac{1}{\sqrt{\pi\tau}}-\frac{u(2\sigma/v+1)}{2\sqrt{R_mD_m}}\right.$$
$$\left.\times\exp\left(\left(\sqrt{\frac{R_m}{D_m}}\frac{z}{2\sqrt{\tau}}+\frac{u(2\sigma/v+1)}{2\sqrt{R_mD_m}}\sqrt{\tau}\right)^2\right)\operatorname{erfc}\left[\sqrt{\frac{R_m}{D_m}}\frac{z}{2\sqrt{\tau}}+\frac{u(2\sigma/v+1)}{2\sqrt{R_mD_m}}\sqrt{\tau}\right]\right\} \quad \text{(B23)}$$

By noting that $\mathfrak{L}^{-1}\{1/(p+a_1)\}=e^{-a_1t}$, then the inverse transform of Eq. (B11) is given by

$$C_m(z,t)=\frac{M_o}{\theta_m\sqrt{R_mD_m}}f(z,t)+\frac{\mu_1C^*}{\theta_m\sqrt{R_mD_m}}\times\int_0^t e^{-a_1(t-\tau)}f(z,\tau)\mathrm{d}\tau \quad \text{(B24)}$$

In its current form and from the definition of $f(z,\tau)$. This equation requires double integration. Fortunately, it can be reduced to a single integral by, firstly, substituting Eq. (B22) for $f(z,\tau)$ in Eq. (B24), and commuting the order of integration; i.e. $\int_0^t\int_0^\tau(\,)\,\mathrm{d}\eta\,\mathrm{d}\tau=\int_0^t\int_\eta^t(\,)\mathrm{d}\tau\mathrm{d}\eta$, and secondly, by using the transformation $\lambda=\tau-\eta$, $\mathrm{d}\lambda=\mathrm{d}\tau$, and the fact that

$$\frac{\mathrm{d}}{\mathrm{d}\lambda}I_0\left[\frac{2\alpha}{\sqrt{\beta R_{im}R_m}}\sqrt{\eta\lambda}\right]=\frac{\alpha}{\sqrt{\beta R_{im}R_m}}\sqrt{\eta/\lambda}I_1\left[\frac{2\alpha}{\sqrt{\beta R_{im}R_m}}\sqrt{\eta\lambda}\right] \quad \text{(B25)}$$

Thus,

$$\int_0^t e^{-a_1(t-\tau)}f(z,\tau)\mathrm{d}\tau=\int_0^t g_1(z,\eta)e^{-a_1(t-\eta)}\times I_0\left[\frac{2\alpha}{\sqrt{\beta R_{im}R_m}}\sqrt{\eta(t-\eta)}\right]\times e^{-(K-a_1)(t-\eta)}\mathrm{d}\eta+(K-a_1)\times\int_0^t e^{-a_1(t-\eta)}g_1(z,\eta)\left\{\int_0^{t-\eta}I_0\left[\frac{2\alpha}{\sqrt{\beta R_{im}R_m}}\sqrt{\eta\lambda}\right]\times e^{-(K-a_1)\lambda}\mathrm{d}\lambda\right\}\mathrm{d}\eta \quad \text{(B26)}$$

The inner integral can be evaluated by parts with the aid of the following Bessel's identity (Wylie and Barrett, 1982):

$$\frac{\mathrm{d}}{\mathrm{d}\lambda}\{(a^2\lambda)^{-u/2}I_u[a\sqrt{\lambda}]\}=\frac{a^{-u+1}}{2}(\sqrt{\lambda})^{-u-1}I_{u+1}[a\sqrt{\lambda}] \quad \text{(B27)}$$

and the use of the following limits:

$$\lim_{\lambda\to0}\frac{I_1[a\sqrt{\lambda}]}{a\sqrt{\lambda}}=\frac{1}{2},\quad\text{and}\quad\lim_{\lambda\to0}\frac{I_2[a\sqrt{\lambda}]}{a^2\lambda}=\frac{1}{8} \quad \text{(B28)}$$

which follows from the definition of the modified Bessel functions. $I_u[x]$ is the modified Bessel function of the first kind of order u. Thus,

$$(K-a_1)\int_0^{t-\eta}I_0\left[\frac{2\alpha}{\sqrt{\beta R_{im}R_m}}\sqrt{\eta\lambda}\right]e^{-(K-a_1)\lambda}\mathrm{d}\lambda=\left\{1+\frac{a^2}{4(K-a_1)}+\frac{1}{2}\left(\frac{a^2}{4(K-a_1)}\right)^2+\cdots\right\}-e^{-(K-a_1)(t-\eta)}\left\{I_0[a\sqrt{t-\eta}+\frac{a}{2(K-a_1)}\frac{I_1[a\sqrt{t-\eta}]}{\sqrt{t-\eta}}+\left(\frac{a}{2(K-a_1)}\right)^2\frac{I_2[a\sqrt{t-\eta}]}{t-\eta}+\cdots\right\} \quad \text{(B29)}$$

in which $a=2(\alpha/\sqrt{\beta R_{im}R_m})\sqrt{\eta}$. By inspection, the first three terms of the first series between parentheses constitute the leading three terms in Taylor expansion of $\exp\{a^2/[4(K-a_1)]\}$, and Eq. (B29) now can be written in a more compact form:

$$(K-a_1)\int_0^{t-\eta}I_0\left[\frac{2\alpha}{\sqrt{\beta R_{im}R_m}}\sqrt{\eta\lambda}\right]e^{-(K-a_1)\lambda}\mathrm{d}\lambda=\exp\left(\frac{\alpha^2}{\beta R_{im}R_m(K-a_1)}\eta\right)-e^{-(K-a_1)(t-\eta)}\times\sum_{n=0}^{\infty}\left[\frac{\alpha^2}{\beta R_{im}R_m(K-a_1)^2}\frac{\eta}{t-\eta}\right]^{n/2}\times I_n\left[\frac{2\alpha}{\sqrt{\beta R_{im}R_m}}\sqrt{(t-\eta)\eta}\right] \quad \text{(B30)}$$

Thus,

$$(K-a_1)\int_0^t e^{-a_1(t-\eta)}g_1(z,\eta)\int_0^{t-\eta} I_0\left[\frac{2\alpha}{\sqrt{\beta R_{\rm im}R_{\rm m}}}\sqrt{\eta\lambda}\right]e^{-(K-a_1)\lambda}\mathrm{d}\lambda\,\mathrm{d}\eta$$
$$=\int_0^t \exp\left(\frac{\alpha^2/R_{\rm m}}{\beta R_{\rm im}(k_{\rm im}-a_1)+\alpha}\eta-a_1(t-\eta)\right)g_1(z,\eta)\left\{1-\exp\left(-\frac{\alpha^2/R_{\rm m}}{\beta R_{\rm im}(k_{\rm im}-a_1)+\alpha}\eta-(K-a_1)(t-\eta)\right)\right.$$
$$\left.\times\sum_{n=0}^{\infty}\left[\frac{\alpha^2}{\beta R_{\rm im}R_{\rm m}(K-a_1)^2}\frac{\eta}{t-\eta}\right]^{n/2} I_n\left[\frac{2\alpha}{\sqrt{\beta R_{\rm im}R_{\rm m}}}\sqrt{(t-\eta)\eta}\right]\right\}\mathrm{d}\eta \tag{B31}$$

The use of Eqs. (B31) in (B26) should lead to

$$\int_0^t e^{-a_1(t-\tau)}f(z,\tau)\mathrm{d}\tau=\int_0^t e^{-a_1(t-\eta)}h_1(z,\eta)\psi(\eta)\mathrm{d}\eta \tag{B32}$$

where

$$h_1(z,\tau)=\exp\left(-\left[k_{\rm m}+\frac{\beta\alpha R_{\rm im}(k_{\rm im}-a_1)/R_{\rm m}}{\alpha+\beta R_{\rm im}(k_{\rm im}-a_1)}\right]\tau\right)h^*(z,\tau) \tag{B33}$$

$$h^*(z,\tau)$$
$$=\exp\left(-\frac{R_{\rm m}}{4D_{\rm m}\tau}\left(\frac{u}{R_{\rm m}}\tau-z\right)^2\right)\left\{\frac{1}{\sqrt{\pi\tau}}-\frac{u(2\sigma/v+1)}{2\sqrt{D_{\rm m}R_{\rm m}}}\right.$$
$$\times\exp\left(\left(\sqrt{\frac{R_{\rm m}}{D_{\rm m}}}\frac{z}{2\sqrt{\tau}}+\frac{u(2\sigma/v+1)}{2\sqrt{D_{\rm m}R_{\rm m}}}\sqrt{\tau}\right)^2\right)$$
$$\left.\times\mathrm{erfc}\left[\sqrt{\frac{R_{\rm m}}{D_{\rm m}}}\frac{z}{2\sqrt{\tau}}+\frac{u(2\sigma/v+1)}{2\sqrt{D_{\rm m}R_{\rm m}}}\sqrt{\tau}\right]\right\} \tag{B34}$$

$$\psi(\tau)$$
$$=1-\exp\left(-\left[\frac{(\alpha^2/R_{\rm m})\tau}{\beta R_{\rm im}(k_{\rm im}-a_1)+\alpha}+(K-a_1)(t-\tau)\right]\right)$$
$$\times\sum_{m=1}^{\infty}\left\{\left(\frac{\alpha^2\tau}{\beta R_{\rm im}R_{\rm m}(K-a_1)^2(t-\tau)}\right)^{m/2}\right.$$
$$\left.\times I_{\rm m}\left[\frac{2\alpha}{\sqrt{\beta R_{\rm im}R_{\rm m}}}\sqrt{(t-\tau)\tau}\right]\right\} \tag{B35}$$

in which $I_{\rm m}[x]$ is the modified Bessel function of the first kind of order m. Finally, substituting Eqs. (B32) in (B24) yields

$$C_{\rm m}(z,t)=\sqrt{\frac{P}{T_{\rm r}}}\frac{M_{\rm o}}{q}f(z,t)+\sqrt{\frac{P}{T_{\rm r}}}\frac{\mu_{\rm l}}{q}$$
$$\times C^*\int_0^t e^{-a_1(t-\tau)}h_1(z,\tau)\psi(\tau)\mathrm{d}\tau \tag{B36}$$

Appendix C

The Laplace transforms of the partial differential Eqs. (12) and (13) are Eqs. (B1) and (B2), subject to Laplace transforms of (45d) and (46),

$$\frac{\mathrm{d}\tilde{C}_{\rm m}}{\mathrm{d}z},\ \frac{\mathrm{d}\tilde{C}_{\rm im}}{\mathrm{d}z}=0,\qquad z\to\infty \tag{C1}$$

$$\theta_{\rm m}\tilde{F}_{\rm m}(0;p)=-\sigma\tilde{C}_{\rm m}(0;p) \tag{C2}$$

Substituting $C^0_{\rm im}$ from Eq. (45a) for $C_{\rm im}(z,0)$, Eq. (B2) can be solved for $\tilde{C}_{\rm im}(z;p)$,

$$\tilde{C}_{\rm im}(z;p)=\frac{\alpha}{\beta R_{\rm im}(p+k_{\rm im})+\alpha}\tilde{C}_{\rm m}(z;p)$$
$$+\frac{\beta R_{\rm im}C^0_{\rm im}}{\beta R_{\rm im}(p+k_{\rm im})+\alpha} \tag{C3}$$

Using Eq. (45a) in Eq. (B1) yields

$$\frac{\mathrm{d}^2\tilde{C}_{\rm m}(z;p)}{\mathrm{d}z^2}-\frac{u}{D_{\rm m}}\frac{\mathrm{d}\tilde{C}_{\rm m}(z;p)}{\mathrm{d}z}$$
$$-\frac{R_{\rm m}}{D_{\rm m}}\left\{p+k_{\rm m}+\frac{1}{R_{\rm m}}\frac{\beta R_{\rm im}(p+k_{\rm im})\alpha}{\beta R_{\rm im}(p+k_{\rm im})+\alpha}\right\}\tilde{C}_{\rm m}(z;p)$$
$$=-\frac{R_{\rm m}C^0_{\rm m}}{D_{\rm m}}-\frac{\beta R_{\rm im}}{D_{\rm m}}\frac{\alpha C^0_{\rm im}}{\alpha+\beta R_{\rm im}(p+k_{\rm im})} \tag{C4}$$

This equation is a linear nonhomogeneous ordinary differential equation whose solution can be expressed as the sum of a particular solution and the solution of

the corresponding homogenous equation,

$$\tilde{C}_{\mathrm{m}}(z;p)=c_1 e^{m_1(p)z}+\frac{C^0_{\mathrm{m}}}{\kappa+s(p)}+\frac{\alpha C^0_{\mathrm{im}}}{R_{\mathrm{m}}(K+p)(\kappa+s(p))} \tag{C5}$$

where

$$\kappa=k_{\mathrm{m}}+\frac{\alpha}{R_{\mathrm{m}}}-K \tag{C6}$$

$s(p)$ is given by Eq. B(13); and c_1 is a constant to be determined by imposing the flux boundary condition (C2). Boundary condition (C1) is used to obtain the homogeneous solution, which is given by the first term on the right-hand-side of Eq. (C5). The second and third terms correspond to a particular solution of Eq. (C4). The use of boundary flux Eq. (C2) with Eq. (C5) leads to

$$\tilde{C}_{\mathrm{m}}(z,p)=-\frac{(\sigma+v)}{\theta_{\mathrm{m}}\sqrt{R_{\mathrm{m}}D_{\mathrm{m}}}}\left\{C^0_{\mathrm{m}}\tilde{\Phi}_1(p)+C^0_{\mathrm{im}}\tilde{\Phi}_2(p)\right\}\times\tilde{f}(z;p)+\left\{C^0_{\mathrm{m}}\tilde{\Phi}_1(p)+C^0_{\mathrm{im}}\tilde{\Phi}_2(p)\right\} \tag{C7}$$

where

$$\tilde{\Phi}_1(p)=\frac{1}{\kappa+s(p)} \tag{C8}$$

$$\tilde{\Phi}_2(p)=\frac{\alpha}{R_{\mathrm{m}}}\frac{1}{(K+p)(\kappa+s(p))} \tag{C9}$$

in which $s(p)$ and $\tilde{f}(z;p)$, respectively, are given by Eqs. (B13) and (B12). Laplace inverse of Eq. (C7) is

$$C_{\mathrm{m}}(z,t)=-\frac{\sigma+v}{\theta_{\mathrm{m}}\sqrt{R_{\mathrm{m}}D_{\mathrm{m}}}}\int_0^t\left[C^0_{\mathrm{m}}\Phi_1(t-\tau)+C^0_{\mathrm{im}}\Phi_2(t-\tau)\right]\times f(z,\tau)\mathrm{d}\tau+C^0_{\mathrm{m}}\Phi_1(t)+C^0_{\mathrm{im}}\Phi_2(t) \tag{C10}$$

where (Roberts and Kaufman, 1966)

$$\Phi_1^{(t)}=\mathfrak{L}^{-1}\left\{\frac{1}{\kappa+s(p)}\right\}=e^{-Kt}\mathfrak{L}^{-1}\left\{\frac{p}{p^2+\kappa p+a}\right\}=e^{-Kt}\frac{r_1e^{r_1t}-r_2e^{r_2t}}{r_1-r_2},\ r_{1,2}=-\frac{\kappa}{2}\pm\frac{1}{2}\sqrt{\kappa^2-4a} \tag{C11}$$

in which a is given by (B14). The Laplace inverse transform of $\tilde{\Phi}_2(p)$ is

$$\Phi_2(t)=\frac{\alpha}{R_{\mathrm{m}}}e^{-Kt}\mathfrak{L}^{-1}\left\{\frac{1}{p^2+\kappa p+a}\right\}=\frac{\alpha}{R_{\mathrm{m}}}e^{-Kt}\frac{e^{r_1t}-e^{r_2t}}{r_1-r_2},\quad r_{1,2}=-\frac{\kappa}{2}\pm\frac{1}{2}\sqrt{\kappa^2-4a} \tag{C12}$$

The solution in the form shown in Eq. (C10) requires double integration. Similarly, it can be reduced into a single integral by substituting Eqs. (C11) and (C12) for $\Phi_1(t)$ and $\Phi_2(t)$, respectively, into Eq. (C10), and using Eq. (B32), obtained in Appendix B, to yield this solution

$$C_{\mathrm{m}}(z,t)=-\frac{\sigma+q}{\theta_{\mathrm{m}}\sqrt{R_{\mathrm{m}}D_{\mathrm{m}}}}\left\{C^0_{\mathrm{m}}\Psi_1(z,t)+C^0_{\mathrm{im}}\Psi_2(z,t)\right\}+C^0_{\mathrm{m}}\Phi_1(t)+C^0_{\mathrm{im}}\Phi_2(t) \tag{C13}$$

where

$$\Psi_1(z,t)=\frac{r_1}{r_1-r_2}\int_0^t e^{-(K-r_1)(t-\tau)}h_1(z,\tau;a_1=K-r_1)\times\psi(\tau;a_1=K-r_1)\mathrm{d}\tau-\frac{r_2}{r_1-r_2}\times\int_0^t e^{-(K-r_2)(t-\tau)}h_1(z,\tau;a_1=K-r_2)\times\psi(\tau;a_1=K-r_2)\mathrm{d}\tau \tag{C14}$$

$$\Psi_2(z,t)=\frac{\alpha}{R_{\mathrm{m}}}\frac{1}{r_1-r_2}\left\{\int_0^t e^{-(K-r_1)(t-\tau)}h_1(z,\tau;a_1=K-r_1)\times\psi(\tau;a_1=K-r_1)\mathrm{d}\tau-\int_0^t e^{-(K-r_2)(t-\tau)}\times h_1(z,\tau;a_1=K-r_2)\psi(\tau;a_1=K-r_2)\mathrm{d}\tau\right\} \tag{C15}$$

in which $h_1(z,\tau;a_1=r)$ is given by Eq. (B33) with r substituted for a_1; and $\psi(\tau;a_1=r)$ is given by Eq. (B35) with r substituted for a_1.

References

Abramowitz, M., Stegun, I.A., 1972. Handbook of Mathematical Functions with Formulas, Graphs, and Mathematical Tables, Dover Publications, New York, 1046 pp.

Batterman, S., Kulshrestha, A., Cheng, H.-Y., 1995. Hydrocarbon vapor transport in low moisture soils. Environ. Sci. Technol. 29, 171–180.

Brusseau, M.L., 1992. Nonequilibrium transport of organic chemicals: the impact of pore-water velocity. J. Contaminant. Hydrol. 9, 353–368.

Brusseau, M.L., 1991. Transport of organic chemicals by gas advection in structured or heterogeneous porous media: development of a model and application to column experiments. Water Resour. Res. 27 (12), 3189–3199.

Brusseau, M.L., Jessup, R.E., Rao, P.S.C., 1989. Modeling the transport of solutes influenced by multiprocess nonequilibrium. Water Resour. Res. 25 (9), 1971–1988.

Choy, B., Reible, D.D., 2000. Diffusion Models of Environmental Transport, CRC Press, Boca Raton, pp. 183.

Coats, K.H., Smith, B.D., 1964. Dead-end pore volume and dispersion in porous media. Soc. Petroleum Engng J. 4, 73–84.

DeSmedt, F., Wierenga, P.J., 1984. Solute transfer through columns of glass beads. Water Resour. Res. 20, 225–232.

Gaudet, J.P., Jegat, H., Vachaud, G., Wierenga, P.J., 1977. Solute transfer, with exchange between mobile and stagnant water, through unsaturated sand. Soil Sci. Soc. Am. J. 41 (4), 665–671.

Gierke, J.S., Hutzler, N.J., McKenzie, D.B., 1992. Vapor transport in unsaturated soil columns: implications for vapor extraction. Water Resour. Res. 28 (2), 323–335.

Gierke, J., Hutzler, N.J., Crittenden, C., 1990. Modeling the movement of volatile organic chemicals in columns of unsaturated soil. Water Resour. Res. 26 (7), 1529–1547.

Gillham, R.W., Sudicky, E.A., Cherry, J.A., Frind, O., 1984. An advection–diffusion concept for solute transport in heterogeneous unconsolidated geological deposits. Water Resour. Res. 20 (3), 369–378.

Govindaraju, R.S., Kavvas, M.L., Jones, S.E., Rolston, E., 1996. Use of Green-Ampt model for analyzing one-dimensional transport in unsaturated soils. J. Hydrol. 178, 337–350.

Grisak, G.E., Pickens, J.F., 1981. An analytical solution for solute transport through fractured media with matrix diffusion. J. Hydrol. 52, 47–57.

Grisak, G.E., Pickens, J.F., 1980. Solute transport through fractured media 1. The effect of matrix diffusion. Water Resour. Res. 16 (4), 719–730.

Güven, O., Molz, F.J., Melville, G., 1984. An analysis of dispersion in a stratified aquifer. Water Resour. Res. 20 (10), 1337–1354.

Haggerty, R., Gorelick, S.M., 1995. Multiple-rate mass transfer for modeling diffusion and surface reactions in media with pore-scale heterogeneity. Water Resour. Res. 31 (10), 2383–2400.

Hantush, M.M., Govindaraju, R.S., Mariño, M.A., Zhang, Z., 2002. Screening model for volatile pollutants in dual porosity soils. J. Hydrol. 260, 58–74.

Hantush, M.M., Mariño, M.A., 1998a. Interlayer diffusive transfer and transport of contaminants in stratified formation. I: theory. J. Hydrologic Engng, ASCE 3 (4), 232–240.

Hantush, M.M., Mariño, M.A., 1998b. Interlayer diffusive transfer and transport of contaminants in stratified formation. II: analytical solutions. J. Hydrologic Engng, ASCE 3 (4), 241–247.

Hutzler, N.J., Gierke, J.S., Krause, L.C., 1989. Movement of Volatile Organic Chemicals in Soils, SSSA Special Publication No. 22, pp. 373–403.

Johnson J.A., Parcher M.A., Parker J.C., Seaton W.J., 1996. VOC vapor transport: implications for risk assessment. Proceedings of the Petroleum Hydrocarbons and Organic Chemicals in Ground Water: Prevention, Detection, and Remediation Conference, November 13–15, Houston, Texas

Jury, W.A., Spencer, W.F., Farmer, W.J., 1983. Behavior assessment model for trace organics in soil: I. model description. J. Environ. Qual. 12 (4), 558–564.

Li, L., Barry, D.A., Culligan-Hensley, P.J., Bajracharya, K., 1994. Mass transfer in soils with local stratification of hydraulic conductivity. Water Resour. Res. 30 (11), 2891–2900.

Lindstrom, F.T., Stone, W.M., 1974. On the start up or initial phase of linear mass transport of chemicals in a water saturated sorbing porous medium. SIAM J. Appl. Math. 26 (3), 578–591.

Lindstrom, F.T., Narasimham, M.N.L., 1973. Mathematical theory of a kinetic model for dispersion of previously distributed chemicals in a sorbing porous medium. SIAM J. Appl. Math. 24 (4), 496–510.

Piquemal, J., 1993. On the modeling conditions of mass transfer in porous media presenting capacitance effects by a dispersion–convection equation for the mobile fluid and diffusion equation for the stagnant fluid. Transport Porous Media 10, 271–283.

Rao, P.S.C., Jessup, R.E., Rolston, D.E., Davidson, J.M., Kilcrease, D.P., 1980. Experimental and mathematical description of nonadsorbed solute transfer by diffusion in spherical aggregates. Soil Sci. Soc. Am. J. 44, 684–688.

Rasmuson, A., Neretnieks, I., 1980. Exact solution of a model for diffusion in particles and longitudinal dispersion in packed beds. AIChE J. 26, 686–690.

Roberts, G.E., Kaufman, H., 1966. Table of Laplace Transforms, W.B. Saunders Company, London, pp. 367.

Shapiro, A.M., 1987. Transport Equations for Fractured Porous Media. Advances in Transport Phenomena in Porous Media, NATO ASI Series, Martinus Nijhoff Publishers, Dordrecht, pp. 405–471.

Sudicky, E.A., Gillham, R.W., Frind, E.O., 1985. Experimental investigation of solute transport in stratified porous media. 1. The non-reactive case. Water Resour. Res. 21 (7), 1035–1041.

Tang, D.H., Frind, E.O., Sudicky, E.A., 1981. Contaminant transport in fractured porous media: analytical solution for a single fracture. Water Resour. Res. 17 (3), 555–564.

Tang, Yi, Aral, M.M., 1992. Contaminant transport in layered porous media 1. General solution. Water Resour. Res. 28 (5), 1389–1397.

Valocchi, A.J., 1985. Validity of local equilibrium assumptions for modeling sorbing solute transport through homogeneous soils. Water Resour. Res. 21 (6), 808–820.

van Genuchten, M.Th., Wagenet, R.J., 1989. Two-site/two-region models for pesticide transport and degradation: theoretical

development and analytical solutions. Soil Sci. Soc. Am. Proc. 53 (5), 1303–1310.

van Genuchten, M.T., Wierenga, P.J., 1976. Mass transfer studies in sorbing porous media I. Analytical solutions. Soil Sci. Soc. Am. Proc. 40 (4), 473–480.

Yates, S.R., Spencer, W.F., Cliath, M.M., 1993. Comparison between measured and predicted rates of pesticide volatilization from an agricultural field. Environ. Impact Agri. Activities 2, 203–215.

Yates, S.R., Papiernik, S.K., Gao, F., Gan, J., 2000. Analytical solutions for the transport of volatile organic chemicals in unsaturated layered systems. Water Resour. Res. 36 (8), 1993–2000.

Wylie, C.R., Barrett, L.C., 1982. Advanced Engineering Mathematics, McGraw-Hill, New York, pp. 1103.

Zaidel, J., Russo, D., Feldman, G., 1996. Theoretical analysis of the impact of vapor transport on the NAPL distribution in dry soils. Adv. Water Resour. 19 (3), 145–162.